AD-A086 835   ANALYTIC SCIENCES CORP READING MA   F/G 8/5
               A FAST ESTIMATION ALGORITHM FOR TWO-DIMENSIONAL GRAVITY DATA (G--ETC(U)
               NOV 79 K S TAIT   F19628-77-C-0152
UNCLASSIFIED   TASC-TR-868-1-1   AFGL-TR-80-0016   NL

1 OF 1
AD
AC86835

END

DATE
FILMED

8-80
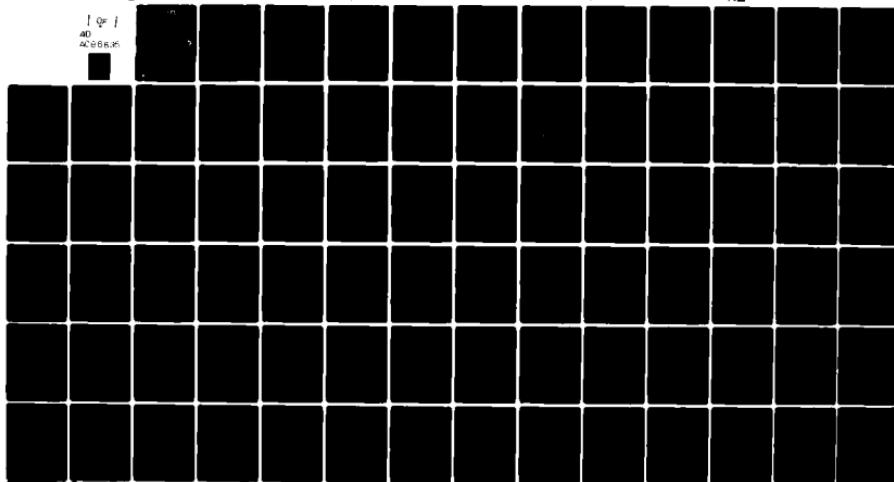
DTIC

AFGL-TR-80-0016

LEVEL

A FAST ESTIMATION ALGORITHM FOR
TWO-DIMENSIONAL GRAVITY DATA (GEOFAST)

Kevin S. Tait

The Analytic Sciences Corporation
Six Jacob Way
Reading, Massachusetts 01867

15 November 1979

DTIC
ELECTE
JUL 1 8 1980

C

Scientific Report No. 2

Approved for public release; distribution unlimited

AIR FORCE GEOPHYSICS LABORATORY
AIR FORCE SYSTEMS COMMAND
UNITED STATES AIR FORCE
HANSCOM AFB, MASSACHUSETTS 01731

80 7 16 012

REPORT DOCUMENTATION PAGE		READ INSTRUCTIONS BEFORE COMPLETING FORM
1. REPORT NUMBER AFGL-TR-80-0016	2. GOVT ACCESSION NO. AD-A086 835	3. RECIPIENT'S CATALOG NUMBER
4. TITLE (and Subtitle) A FAST ESTIMATION ALGORITHM FOR TWO-DIMENSIONAL GRAVITY DATA (GEOFAST)		5. TYPE OF REPORT & PERIOD COVERED Scientific Report No. 2
		6. PERFORMING ORG. REPORT NUMBER TASC-TR-868-1-1, SCIENTIFIC-2
7. AUTHOR(s) Kevin S. Tait		8. CONTRACT OR GRANT NUMBER(s) F19628-77-C-0152
9. PERFORMING ORGANIZATION NAME AND ADDRESS The Analytic Sciences Corporation Six Jacob Way Reading, Massachusetts 01867		10. PROGRAM ELEMENT, PROJECT, TASK AREA & WORK UNIT NUMBERS 32042AA
11. CONTROLLING OFFICE NAME AND ADDRESS Air Force Geophysics Laboratory Hanscom AFB, Massachusetts 01731 Monitor/Lt. Col. Norman H. Mason/LWG		12. REPORT DATE 15 November 1979
		13. NUMBER OF PAGES 84
14. MONITORING AGENCY NAME & ADDRESS(if different from Controlling Office)		15. SECURITY CLASS. (of this report) Unclassified
		15a. DECLASSIFICATION/DOWNGRADING SCHEDULE

16. DISTRIBUTION STATEMENT (of this Report)

Approved for public release; distribution unlimited.

17. DISTRIBUTION STATEMENT (of the abstract entered in Block 20, if different from Report)

18. SUPPLEMENTARY NOTES

19. KEY WORDS (Continue on reverse side if necessary and identify by block number)

Minimum-Variance Estimation, Two-Dimensional Wiener Filtering, Least-Squares Collocation, GEOFAST, Gravity Anomalies, Geoid Heights, Statistical Gravity Models

20. ABSTRACT (Continue on reverse side if necessary and identify by block number)

This report describes an algorithm for the efficient computation of minimum-variance estimates from large amounts of two-dimensional gravity data. The method (called GEOFAST for "geodetic fast estimation") is based on the fast Fourier transform and takes advantage of the underlying structure of the statistical models in the frequency domain. An approximate

DD FORM 1473 EDITION OF 1 NOV 65 IS OBSOLETE

LOG sub 2

ABSTRACT (Continued)

solution is obtained in a number of computer operations proportional to $N\log_2 N$, where N is the number of data points and the proportionality constant is controlled by the desired level of accuracy. Results are presented from two test cases, using GEOS-3 radar altimeter data to estimate mean gravity anomalies, which verify the efficiency and accuracy of the algorithm.

ABSTRACT

This report describes an algorithm for the efficient computation of minimum-variance estimates from large amounts of two-dimensional gravity data. The method (called GEOFAST for "geodetic fast estimation") is based on the fast Fourier transform and takes advantage of the underlying structure of the statistical models in the frequency domain. An approximate solution is obtained in a number of computer operations proportional to $Nlog_2N$, where N is the number of data points and the proportionality constant is controlled by the desired level of accuracy. Results are presented from two test cases, using GEOS-3 radar altimeter data to estimate mean gravity anomalies, which verify the efficiency and accuracy of the algorithm.

TABLE OF CONTENTS

5

LIST OF FIGURES

LIST OF TABLES

1. INTRODUCTION

Large amounts of surface gravity data now exist in organizations such as the Department of Defense (DoD) Gravity Library located at the Defense Mapping Agency Aerospace Center (DMAAC). Present holdings are expected to increase substantially in the future as data from other sophisticated sensor technologies become available. Such sensors include satellite radar altimeters, satellite-to-satellite tracking instrumentation, and airborne gravity gradiometers. For example, DMAAC holdings of GEOS-3 satellite radar altimeter along-track geoid heights were more than one million points in 1978 even after smoothing to a 1 sec data rate (Ref. 3).

Many applications require an accurate estimation of the earth's gravitational field from the existing partial-earth-coverage gravity information. In particular, precise values of the gravity disturbance vector are needed for the compensation of modern inertial guidance and navigation systems. An attractive and widely-known technique is statistical minimum-variance estimation (or "least-squares collocation"). This method has optimal properties with respect to the assumed models, and is easily adapted to a wide class of problems (Refs. 9 and 17). The major inhibitor to the widespread application of optimal gravity data processing is the severe computer time and storage demand when used with high-density gravity surveys.

This report describes an algorithm, GEOFAST, which provides a significant reduction in the computational cost of statistically optimal methods as applied to gravity data estimation.

11

The concept exploits the special structure of gravity model covariance functions, together with the computational efficiency of the Fast Fourier Transform (Refs. 4 and 5), to achieve a computational complexity of order $N\log_2 N$.* The result is an estimation technique which is suitable for processing very large gravity databases. In contrast, standard methods have a complexity of order N^3, and the best competing algorithm, due to Levinson (Refs. 1, 14, 16, and 23), is of order N^2 complexity. For 1000 data points such methods are up to 100 times more expensive than the present technique in terms of computer time.

The basic frequency domain approach of Generalized Wiener Filtering (Refs. 18 and 22) assumes planar data of infinite extent, and results in low accuracy when truncated to finite data sets. An extension to this method suitable for finite track lengths in one-dimensional estimation was described in Ref. 10. The error properties of the proposed method were analyzed in detail and shown to be superior to the basic technique, while retaining the same order of complexity. This method, called GEOFAST for "geodetic fast estimation", was refined and implemented using simulated along-track gravity data with good results (Ref. 21). <u>The algorithm has now been extended to two-dimensions resulting in further refinement and modification, while retaining its accuracy and efficiency properties</u>. A test plan was developed to evaluate the performance of GEOFAST using satellite radar altimeter data from GEOS-3, and has been completed with good results.

This report is organized into four chapters and two appendices. Chapter 2 describes the two-dimensional GEOFAST

---

*Complexity is the functional dependence of the number of multiplications (hence computer time) on the number of data points, N, for large N.

algorithm in outline form with reference to the appendices for details. Appendix A is a brief development of the mathematical theory underlying the one-dimensional version and is a condensation of material in Ref. 10. Appendix B describes the theory necessary to extend the method to two dimensions including a definition of the relevant tensor concepts. The results of two test case applications using GEOS-3 data are presented in Chapter 3, together with performance evaluations. The last chapter, Chapter 4, contains a short summary.

2. THE GEOFAST ALGORITHM

2.1 FORMULATION OF THE PROBLEM

The GEOFAST algorithm was developed to provide an efficient computational solution to the minimum-variance estimation equations

$$\underline{\hat{x}} = C_{xz} \, C_{zz}^{-1} \, \underline{z} \qquad\qquad (2.1\text{-}1)$$

In geodetic work, this formula is commonly known as least-squares collocation (Ref. 9 and 17). Here $\underline{z}$ is a data-vector of dimension N and C_{zz} its auto-covariance matrix of dimension N×N. The vector of estimates $\underline{\hat{x}}$ is of dimension M, and C_{xz} is the cross-covariance matrix between $\underline{x}$ and $\underline{z}$ of dimension M×N. The covariance C_{zz} is generally modelled by an analytic function with parameters fitted to global or local data, and includes measurement noise. The cross-covariance C_{xz} is then analytically derived from C_{zz} by using the physical relationship between the estimated quantities $\underline{x}$ and the observed quantities $\underline{z}$ (Refs. 11, 13, and 24). The method is implicit since this relationship does not appear explicitly via a measurement equation of the form $\underline{z} = H \, \underline{x}$. Formally, the covariances are defined by

$$C_{zz} = E\{\underline{z} \, \underline{z}^T\} \quad , \quad C_{xz} = E\{\underline{x} \, \underline{z}^T\} \qquad\qquad (2.1\text{-}2)$$

where E is the expectation operator and both vectors are assumed to have zero means.

Computer solution of Eq. 2.1-1 by standard techniques involves on the order of N^3 operations (such as multiplications

and additions) to obtain the intermediate vector

$$\underline{u} = C_{zz}^{-1} \underline{z} \qquad (2.1\text{-}3)$$

and on the order of MN operations to yield the estimates

$$\underline{\hat{x}} = C_{xz} \underline{u} \qquad (2.1\text{-}4)$$

This limits the feasible application of these methods to data sets of a few hundred points at most, whereas thousands of measurements are often available from such sensors as satellite altimeters.

By making two assumptions and using frequency domain techniques this workload can be reduced dramatically to the order of $N\log_2 N$. First, let the data points $z(\theta,\phi)$ be given on a rectangular grid in the θ,ϕ plane (Fig. 2.1-1). Second, assume that the covariance between two data points is a function of relative position only. That is, the covariance function is shift-invariant (or a displacement kernel)

$$COV [z(\theta_1,\phi_1), z(\theta_2,\phi_2)] = f_{zz}(\theta_2-\theta_1, \phi_2-\phi_1) \qquad (2.1\text{-}5)$$

Note that this assumption includes, but is not restricted to, the case of isotropic models. Similar assumptions are made for the cross-covariance and estimate points $x(\theta,\phi)$, namely,

$$COV [x(\theta_1,\phi_1), z(\theta_2,\phi_2)] = f_{xz}(\theta_2-\theta_1, \phi_2-\phi_1) \qquad (2.1\text{-}6)$$

where it is here assumed for simplicity that the estimates are obtained on the same grid as the data.

The foregoing assumptions are not unduly restrictive in practice as shown by the application to GEOS-3 data in Chapter 3. Data given on a limited region of a spherical (or

15
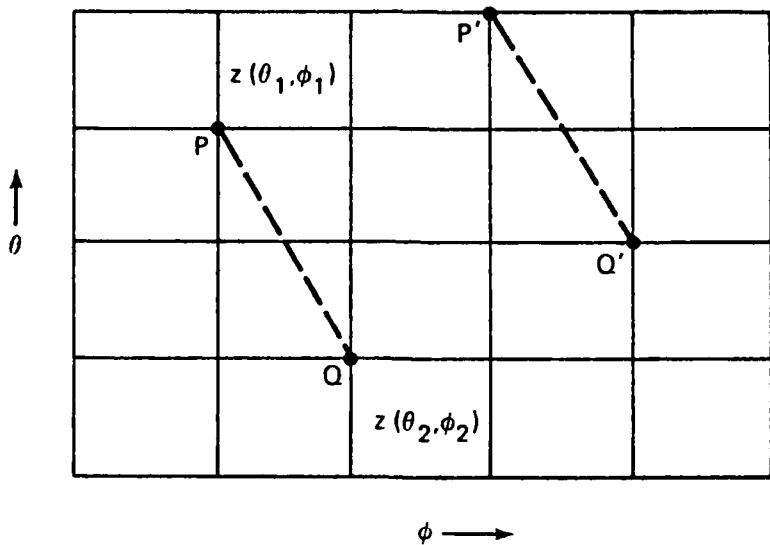
$$\text{COV }(P,Q) = \text{COV }(P',Q') = f_{zz}\,(\theta_2 - \theta_1,\, \phi_2 - \phi_1)$$

Figure 2.1-1   Data and Covariance Structure

ellipsoidal) surface may be mapped onto a plane with very little distance distortion and then gridded. The shift invariance assumption then corresponds to the common model of stationary statistics. The estimate grid may actually be any translation (that is offset in altitude, latitude, and longitude) of the data grid. With a fast algorithm it is often cheaper to compute estimates at all grid locations even if only a subset is wanted.

The stated assumptions give to the estimation Eq. 2.1-1 a special structure which is exploited by the GEOFAST algorithm. The natural form for the data is an $n_1 \times n_2$ matrix

$$Z = [z_{jk}] \quad , \quad z_{jk} = z(\theta_0 + j\Delta\theta,\ \phi_0 + k\Delta\phi) \qquad (2.1\text{-}7)$$

where $j = 0, 1, \ldots, n_1 - 1$ and $k = 0, 1, \ldots, n_2 - 1$ corresponding to the data grid (Fig. 2.1-1) with origin (θ_0, ϕ_0) and mesh size $(\Delta\theta, \Delta\phi)$. The total number of grid points is $N = n_1 n_2$. The data matrix Z is put in vector form $\underline{z}$ by listing its elements in

16

row-by-row order. With this convention the N×N covariance matrix C_{zz} assumes a block structure (see Appendix B)

$$C_{zz} = \begin{bmatrix} T_0 & T_1 & \cdot & \cdot & T_{n_1-1} \\ T_{-1} & T_0 & \cdot & \cdot & T_{n_1-2} \\ \cdot & \cdot & \cdot & \cdot & \cdot \\ T_{-(n_1-1)} & T_{-(n_1-2)} & \cdot & \cdot & T_0 \end{bmatrix} \qquad (2.1-8)$$

in which there are $n_1 \times n_1$ blocks and each block is of dimension $n_2 \times n_2$. The block matrix T_k is the cross-covariance between the elements in two rows of Z which are k rows apart. This depends only on k by shift-invariance. By the same argument each block matrix is of the form

$$T = \begin{bmatrix} t_0 & t_1 & \cdot & \cdot & t_{n_2-1} \\ t_{-1} & t_0 & \cdot & \cdot & t_{n_2-2} \\ \cdot & \cdot & \cdot & \cdot & \cdot \\ t_{-(n_2-1)} & t_{-(n_2-2)} & \cdot & \cdot & t_0 \end{bmatrix} \qquad (2.1-9)$$

The matrix C_{zz} is said to be block Toeplitz with Toeplitz blocks, or simply block Toeplitz. Note that C_{zz} is symmetric and is completely determined by its first block row (or block column), whereas the blocks (except T_0) are not symmetric and are determined by their first row and column. Altogether, the definition of C_{zz} requires less than $2n_1 n_2 = 2N$ parameters. The structure of C_{xz} is the same except that symmetry does not hold in general, so that approximately 4N parameters are needed to define it. In summary, the geodetic estimation problem is equivalent to the inversion and multiplication of block Toeplitz matrices.

2.2 OUTLINE OF THE ALGORITHM

The GEOFAST algorithm achieves its efficiency by transforming the estimation equations into the frequency domain where an accurate approximation can be made to reduce the workload. The transformation is accomplished with the Fast Fourier Transform (FFT) which requires on the order of $N\log_2 N$ operations. The transformed covariance matrices are closely approximated by (block) banded matrices resulting in a solution workload of order N. A simple trade-off between approximation accuracy and computer workload is controllable by choice of the bandwidth.

A simplified flow chart of the algorithm is shown in Fig. 2.2-1. Input to the computation consists of the $n_1 \times n_2$ data matrix Z, together with the definition of the covariance matrices C_{xz}, C_{zz}. As seen in Eqs. 2.1-8 and 2.1-9, each covariance can be specified by $4n_1 n_2$ parameters which are naturally arranged as a $2n_1 \times 2n_2$ correlation matrix. Specifically, let the Toeplitz matrix T in Eq. 2.1-9 be represented by the column vector[*]

$$\underline{t} = \left[0, \; t_{-(n_2-1)}, \; \cdots, \; t_{-1}, \; t_0, \; t_1, \; \cdots, \; t_{n_2-1} \right]^T$$

$$(2.2-1)$$

of dimension $2n_2$. Then each block matrix T_k in Eq. 2.1-8 can be represented by a vector $\underline{t}_k$, and the matrix C_{zz} by the $2n_1 \times 2n_2$ matrix

$$T_{zz} = \left[\underline{0} \; \vdots \; \underline{t}_{-(n_1-1)} \; \vdots \; \cdots \; \vdots \; \underline{t}_{-1} \; \vdots \; \underline{t}_0 \; \vdots \; \underline{t}_1 \; \vdots \; \cdots \; \vdots \; \underline{t}_{n_1-1} \right]^T$$

$$(2.2-2)$$

---

[*]Superscript T is used throughout this report to denote the transpose operator. When not a superscript, T is used to denote a Toeplitz matrix without causing ambiguity.

18
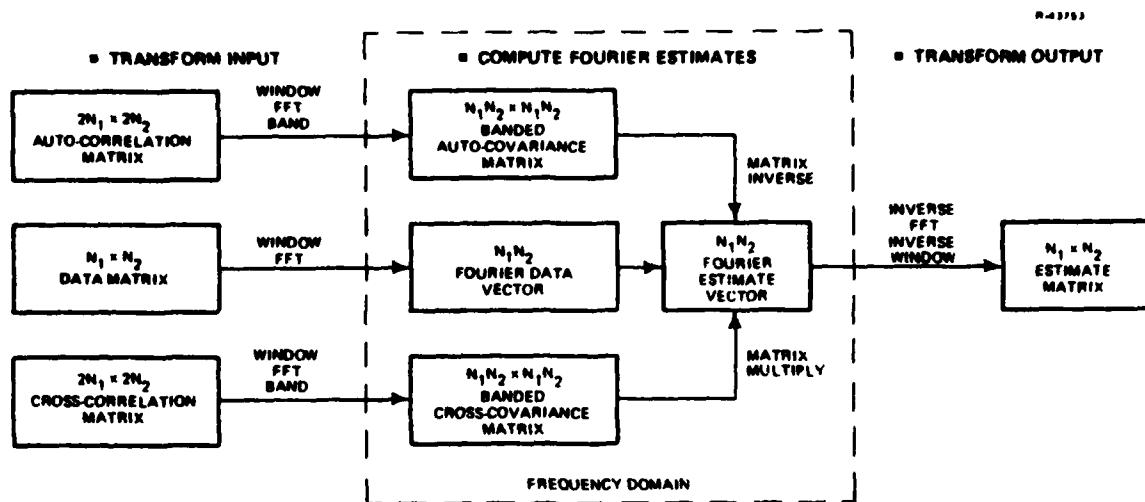
Figure 2.2-1   Two-Dimensional GEOFAST Algorithm

For the symmetric case (C_{zz}), only half of the matrix T_{zz} is
required with $\underline{t}_{-k} \equiv \underline{t}_k$. Total computer storage for input is
of order $N = n_1 n_2$.

2.2.1   Transformation to the Frequency Domain

The first stage of the algorithm is the transformation
of the inputs to the frequency domain.   The FFT is simply an
efficient implementation of the complex Discrete Fourier Trans-
form (DFT) which is defined in two dimensions by*

$$z'_{pq} = \frac{1}{\sqrt{n_1 n_2}} \sum_{j=0}^{n_1} \sum_{k=0}^{n_2} z_{jk} \exp \left\{ -2\pi i \left(\frac{pj}{n_1} + \frac{qk}{n_2} \right) \right\} \quad (2.2\text{-}3)$$

Since the estimation equations, Eq. 2.1-1, are in terms of the
data vector $\underline{z}$ it is convenient to express Eq. 2.2-3 in the
equivalent matrix form,

---

*The symbol i denotes the imaginary unit $\sqrt{-1}$.

$$\underline{z}' = F \underline{z} \qquad\qquad (2.2\text{-}4)$$

The N×N complex two-dimensional DFT matrix F has a special structure which is discussed further in Appendix B. The vector $\underline{z}'$ in Eq. 2.2-4 is the complex representation of the data vector $\underline{z}$ in a finite Fourier series of complex exponentials. Since real quantities are more convenient to deal with in a computer, a further transformation to a sine and cosine series is performed by combining real and imaginary parts. This corresponds to the matrix operations (redefining $\underline{z}'$)

$$\underline{z}' = H F \underline{z} \qquad\qquad (2.2\text{-}5)$$

where H is a very sparse complex N×N matrix. The product HF is, of course, a real matrix.

Finally, the accuracy of the banded approximation, which is essential for the success of the algorithm, is critically enhanced by the introduction of a data window. In matrix form this becomes (redefining $\underline{z}'$ again)

$$\underline{z}' = H F W \underline{z} \qquad\qquad (2.2\text{-}6)$$

where W is a real N×N diagonal matrix. That is, each data value z_{jk} is multiplied by a scalar weight w_{jk} before applying the DFT. This windowing compensates for the finite extent of the data grid in a manner explained in Appendix A. A representative window function in two dimensions would be a gaussian probability density which is peaked at the center and tapered toward the edges of the data grid. In GEOFAST, an optimal one-dimensional window $\underline{w}^O$ derived by Kaiser (Ref. 15) is used to form a product window $w_{jk} = (w_j^O)(w_k^O)$ (Fig. 2.2-2). The combined data transformation in Eq. 2.2-6 can be implemented in order $N\log_2 N$ operations since multiplication by H and W are both order N.

R-49248
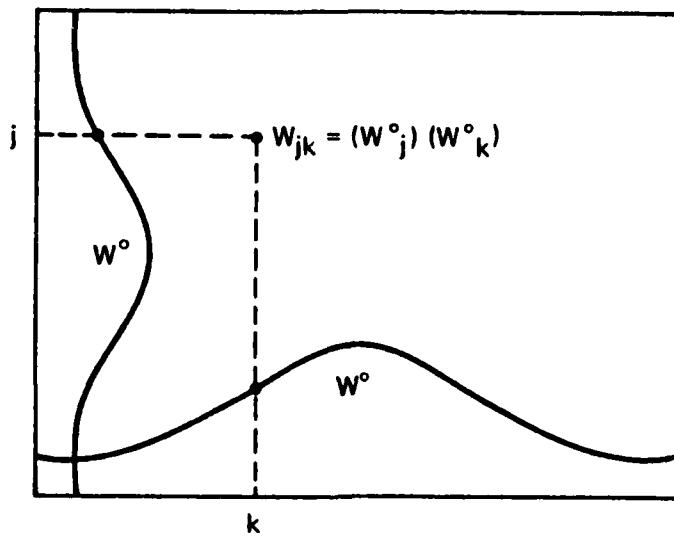
Figure 2.2-2   Product Window Definition

Corresponding to the frequency domain data vector $\underline{z}'$ (consisting of Fourier coefficients) is the auto-covariance matrix

$$C'_{zz} = E\{\underline{z}'(\underline{z}')^T\} = (H\ F\ W)\ C_{zz}\ (H\ F\ W)^T \qquad (2.2\text{-}7)$$

Similarly, introducing the transformed estimates

$$\hat{\underline{x}}' = (H\ F\ W)\hat{\underline{x}} \qquad (2.2\text{-}8)$$

leads to the cross-covariance matrix

$$C'_{xz} = E\{\underline{x}'(\underline{z}')^T\} = (H\ F\ W)\ C_{xz}\ (H\ F\ W)^T \qquad (2.2\text{-}9)$$

A straightforward row and column implementation of Eqs. 2.2-7 and 2.2-9 would result in an order $N^2 \log_2 N$ algorithm. This is avoided by replacing C'_{xz} and C'_{zz} by their banded approximations, and calculating only those elements within the retained bands. If the number of bands in the one dimensional window is m_B this

21

reduces the workload to the order of $m_B^2 N \log_2 N$, where for typical applications m_B is small and independent of N. The scheme used to compute C'_{xz} and C'_{zz} bandwise is derived in Appendices A and B, and is an essential part of the GEOFAST algorithm.

2.2.2 Solution of the Estimation Equations

The preceding transformations constitute the first stage of the calculation (Fig. 2.2-1). Note that storage requirements for the covariances are of order $m_B^2 N$. The second stage consists of the solution of the estimation equations in the frequency domain. The estimation equations in the transformed variables become simply

$$\underline{\hat{x}}' = C'_{xz}(C'_{zz})^{-1} \underline{z}' \qquad (2.2\text{-}10)$$

coupled with the inverse of Eq. 2.2-8

$$\underline{\hat{x}} = (H\ F\ W)^{-1} \underline{\hat{x}}' \qquad (2.2\text{-}11)$$

It is easily verified that the solution of Eqs. 2.2-10 and 2.2-11 is identical to the solution of Eq. 2.2-1. As before, the equations are solved in two steps

$$\underline{u}' = (C'_{zz})^{-1} \underline{z}' \qquad (2.2\text{-}12)$$

$$\underline{\hat{x}}' = C'_{xz} \underline{u}' \qquad (2.2\text{-}13)$$

Since C'_{xz} is banded, the multiplication in Eq. 2.2-13 requires only on the order of $m_B^2 N$ operations.

However, analysis of the solution of Eq. 2.2-12 is more complicated. It is shown in Appendix B that the block

22

Toeplitz structure of C_{zz} in Eq. 2.1-8 gives rise to a corresponding block-banded structure for C'_{zz} in which the blocks are also banded (Fig. 2.2-3). There is an essential difference between this structure and the simple band structure of a diagonal block which is the one-dimensional analogue of C'_{zz}. In the one-dimensional problem, the symmetric band matrix C'_{zz} can be inverted in order $m_B^2 n$ operations by the standard Cholesky technique (Refs. 6 and 12), where n is the matrix dimension and m_B the number of superdiagonal bands. When the Cholesky technique is applied to the block-banded structure of the two-dimensional problem, the internal banding within the blocks is lost during the calculation. This difficulty is known as "fill-in". The result is an effective bandwidth of $m_B n_2$, where m_B is now the number of blockbands of size $n_2 \times n_2$, and a workload of order $(m_B n_2)^2 (n_1 n_2)$. Assuming $n_1 = n_2$ gives an order of effort proportional to $n_1^4 = N^2$ rather than N.


R-49251
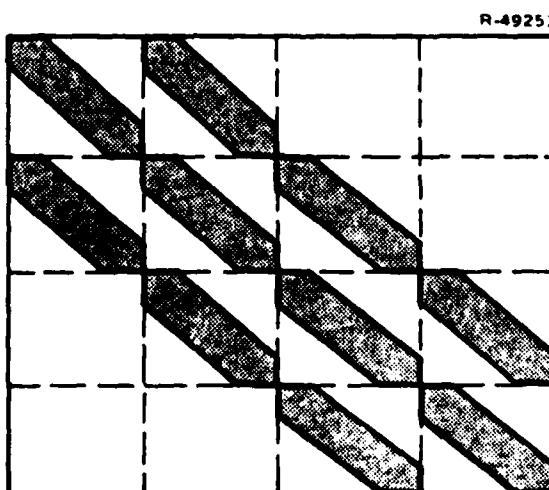
Figure 2.2-3   Block Banded Structure

An order N algorithm for the solution of Eq. 2.2-12 can be developed by using an iterative method based on a special

class of covariance matrices. This special type of covariance structure is termed separable and is characterized by a covariance function in Eq. 2.1-5 of the form

$$f_{zz}(\theta_2 - \theta_1, \phi_2 - \phi_1) = f_1(\theta_2 - \theta_1) \, f_2(\phi_2 - \phi_1) \qquad (2.2-14)$$

This class of functions is not general enough to include the statistical models required for gravimetric applications, but it can serve as an approximation for use in an iterative method. It is shown in Appendix B that for a separable covariance matrix Eq. 2.2-12 "factors" into two one-dimensional matrix equations of the form

$$V' = (C_2')^{-1}(Z')^T \qquad (2.2-15)$$

$$U' = (C_1')^{-1}(V')^T \qquad (2.2-16)$$

where C_1', C_2' correspond to f_1, f_2 and are square band matrices of dimension n_1, n_2. The matrices Z' and U' are both of dimension $n_1 \times n_2$, and are equivalent to the vectors $\underline{z}'$ and $\underline{u}'$ when their elements are listed in row-by-row order. If the bandwidth of the matrix C_2' is m_B, then Eq. 2.2-15 can be solved by the Cholesky method in order $m_B n_2 (m_B + n_1)$ operations. Assuming $n_1 = n_2$, the total workload for both equations is thus of order $m_B N$ in the separable case.

The iterative solution of Eq. 2.2-12 in the non-separable case proceeds as follows. Choose the matrix D' as a separable approximation to C_{zz}' (which may be done in a natural way) and define the matrix E' by

$$C_{zz}' = D' + E' \qquad (2.2-17)$$

The matrix E' will be block-banded since both C_{zz}' and D' are. The estimation equation can now be written implicitly

$$\underline{u}' = (D')^{-1} [\underline{z}' - E'\underline{u}'] \qquad (2.2\text{-}18)$$

or in recursive form

$$\underline{u}'(k+1) = (D')^{-1} [\underline{z}' - E'\underline{u}'(k)] \qquad (2.2\text{-}19)$$

where k indicates the iteration number and $\underline{u}'(0)$ is any convenient initial solution.

Since both the inversion and multiplication in Eq. 2.2-19 require on the order of N operations, so does one step of the iteration. If the number of steps, m_s, necessary for convergence of the iteration is independent of N and small enough, the total workload to solve Eq. 2.2-12 is of order N. It can be shown that the rate of convergence depends on the norm of the matrix $(D')^{-1}E'$ which will be small if the separable approximation is a good one. Furthermore, a simple modification to the iteration guarantees convergence for any positive definite matrix D'. The convergence properties of the iterative technique, Eq. 2.2-19, and the appropriate choice of the approximating matrix D' are discussed in Appendix B.

The solution of the estimation equations in the frequency domain completes the second stage of the GEOFAST algorithm (Fig. 2.2-1). The third stage consists of the inverse transformation back to the space domain (Eq. 2.2-11). Since W is a diagonal matrix, its inverse is an order N operation. The complex DFT matrix F can be inverted in order $N\log_2 N$ operations by means of the inverse FFT, while the inverse of the matrix H can be obtained analytically and has the same sparse structure as H itself. Thus the final stage has a workload dominated by $N\log_2 N$.

25

The computer time and storage requirements for the GEOFAST algorithm are summarized in Table 2.2-1. The numbers given are asymptotic estimates, valid for large N, and do not include multiplicative factors independent of N except for m_B and m_s. For repeated application of the algorithm with the same covariance model, the matrices C'_{xz} and C'_{zz} can be stored, reducing the time requirement to the order of $N\log_2 N$ for each application to a new data set.

TABLE 2.2-1

COMPUTER TIME AND STORAGE REQUIREMENTS

ALGORITHM STAGE	ASYMPTOTIC ORDER OF MAGNITUDE	
	TIME	STORAGE
1: Input Transforms	$m_B^2 N\log_2 N$	$m_B^2 N$
2: Estimation Equations	$m_s m_B^2 N$	$m_B^2 N$
3: Output Transform	$N\log_2 N$	N
Full Solution	$m_B^2 N\log_2 N$	$m_B^2 N$

N = Total number of data points

m_B = Bandwidth in one dimension

m_s = Number of steps for convergence

3.   APPLICATION TO GEOS-3 DATA

        In order to evaluate the GEOFAST technique a Test
Plan was developed in coordination with DMAAC. The objectives
of the plan were to test the effectiveness of GEOFAST when
applied to gravity survey data and to compare accuracy and
efficiency with existing DMAAC methods. It was decided that
GEOS-3 satellite altimeter data would be a natural choice for
the test plan since a large data set existed, and computer
processing time is a critical parameter in the ability to
utilize such information in an optimal manner.

        A 20 deg by 20 deg area in the Atlantic was chosen
from which to process GEOS-3 data. The test area, bounded by
17 deg and 37 deg N latitude and 285 deg and 305 deg E longi-
tude (Fig. 3-1) includes Bermuda and Puerto Rico. Much of the
GEOS-3 calibration area is also included so that the track
density is relatively high. The geoid heights derived from
the altimeter measurements were then used to estimate mean
gravity anomalies. The implementation of the test plan re-
sulted in the two test cases described below.

        The computer program used to generate the test case
results differed in some aspects from the algorithm described
in Chapter 2. The test program utilized a preliminary version
of GEOFAST in which the iterative scheme of Section 2.2.2 was
not operational. An alternative approach was implemented re-
quiring increased computer storage to achieve comparable accu-
racy and efficiency. A full implementation of the GEOFAST
algorithm is currently being developed, and will be subjected
to the same test plan when available.

                              27
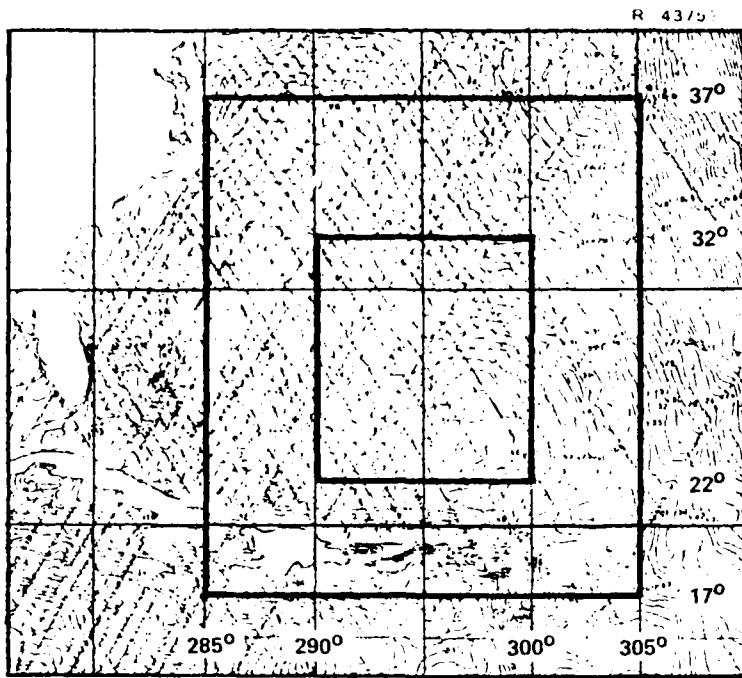
Figure 3-1   GEOS-3 Test Area

3.1   TEST CASE NO. 1

Basic data for this test case were the 1 deg gridded geoid heights derived by DMAAC (Ref. 3) with an estimated accuracy of approximately 1 m. Mean gravity anomaly estimates were obtained on the same 1 deg grid for the central 10 deg by 10 deg square of the test area. Three different algorithms were used to obtain the estimates: GEOFAST, Spatial Collocation, and Inverse Stokes (Ref. 9), the latter two being techniques in use at DMAAC. All algorithms used exactly the same input data so that comparisons could be made, and in the case of GEOFAST and Spatial Collocation the same DMAAC-developed covariances were used.

Two transformations were applied to the basic data to produce the input data for the algorithms. First, a global

spherical harmonic expansion of the geoidal undulation to de-
gree and order 12 was subtracted from the GEOS-3 geoid heights.
These are termed residual GEOS-3 geoid heights and are contour-
plotted in Fig. 3.1-1(a). Second, a "template" approach was
used to generate the estimates. That is, the 10 deg by 10 deg
square for which the mean gravity anomalies are desired was
subdivided into four 5 deg by 5 deg subregions (Fig. 3.1-2).
Within each subregion, only the surrounding 15 deg by 15 deg
square of data was used in forming the estimates[*] (Fig. 3.1-3).
For each 15 deg square, the mean residual geoid height was com-
puted and subtracted from the data to remove bias. The resid-
ual mean gravity anomaly estimates were generated independently
by subregion and combined to yield estimates over the 10 deg
region. To these residual estimates, (Fig. 3.1-1(b)), the
spherical harmonic expansion of the (point) gravity anomaly to
degree and order 12 was added to obtain the final mean gravity
anomaly estimates.

In the statistical methods (GEOFAST and Spatial Col-
location), the covariances for the residual geoid heights and
residual mean gravity anomalies were obtained from the Tscherning-
Rapp model No. 4 (Ref. 24) with terms to degree and order 12
removed. The mean gravity anomalies were modeled as point
anomalies at 10.4 km altitude. (See Ref. 24 for a justifica-
tion of this approximation.) The resulting covariances are
displayed as a function of spherical distance in Fig. 3.1-4.

For an independent reference, the estimated mean grav-
ity anomalies were compared with values from the DoD Gravity
Library obtained by surface gravity surveys. This data base
is on a 5 min grid and was averaged over 1 deg squares to yield
comparison values. Statistics of the comparison are displayed

---

[*]For the Inverse Stokes method, only a 9 deg by 9 deg square
was used.
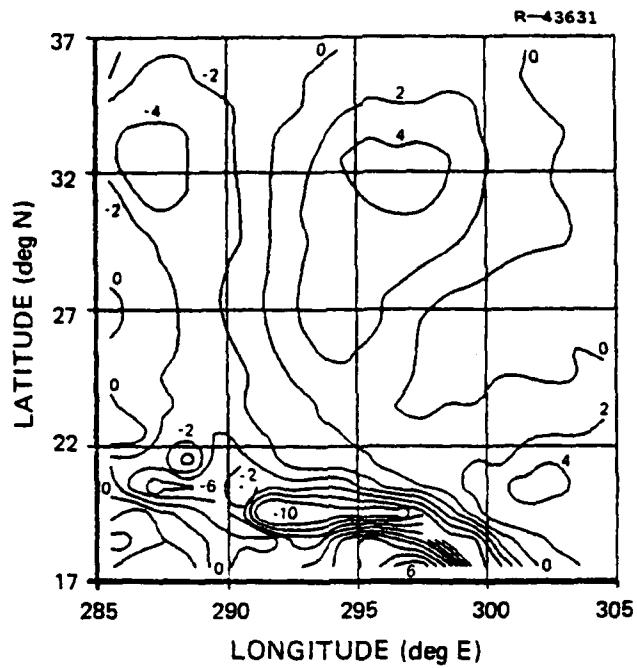
(a) Residual GEOS-3 Geoid Heights (m)
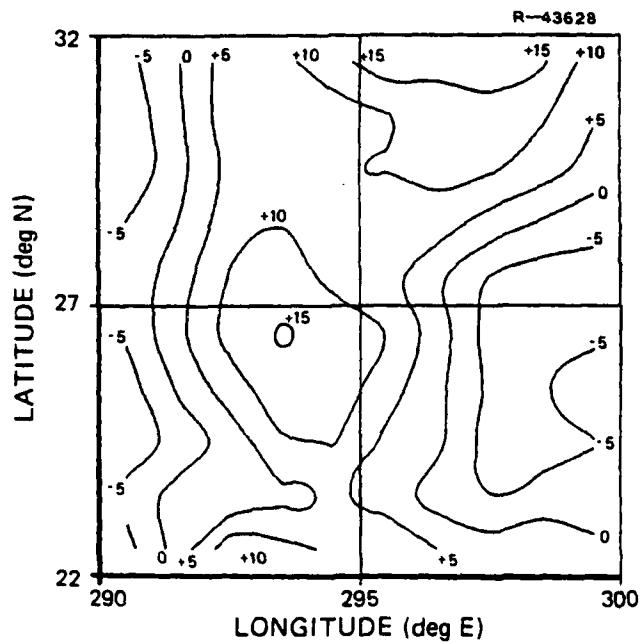
(b) GEOFAST Residual Mean Gravity Anomaly Estimates (mgal)

Figure 3.1-1   Residual GEOS-3 Geoid Heights and GEOFAST
                Residual Mean Gravity Anomaly Estimates
                for Test Case No. 1
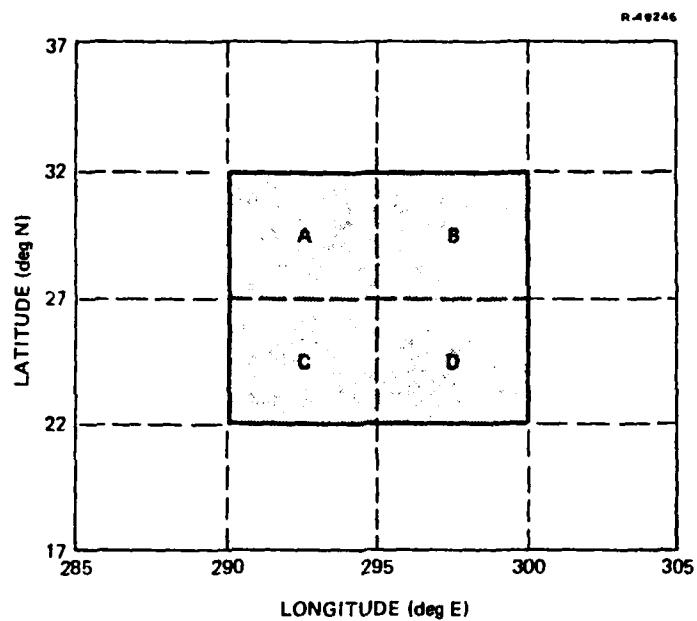
Figure 3.1-2   Subdivision of the Estimation Region
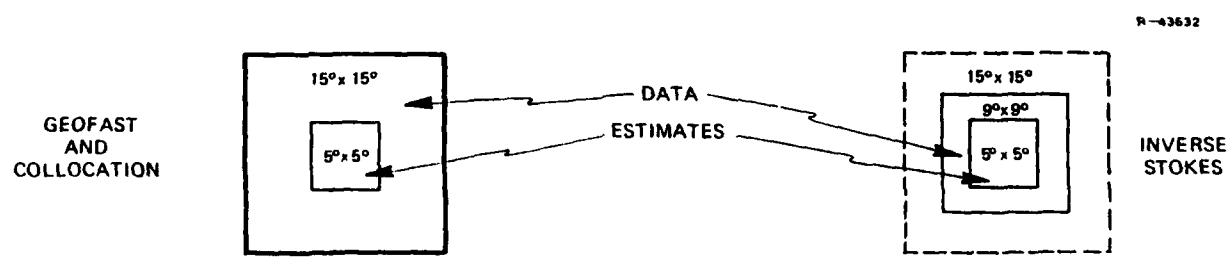
NOTE: IN ALL CASES 15° x 15° RESIDUAL GEOID MEAN SUBTRACTED FROM DATA

Figure 3.1-3   Estimation Templates

31

R-43750
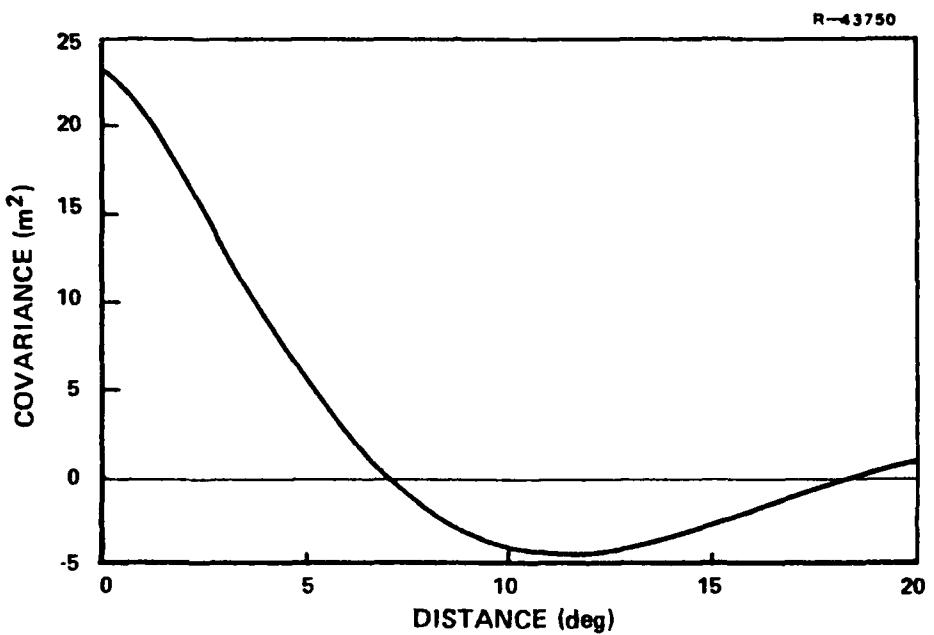
(a)   Residual Geoid Height Auto-Covariance

R-43751
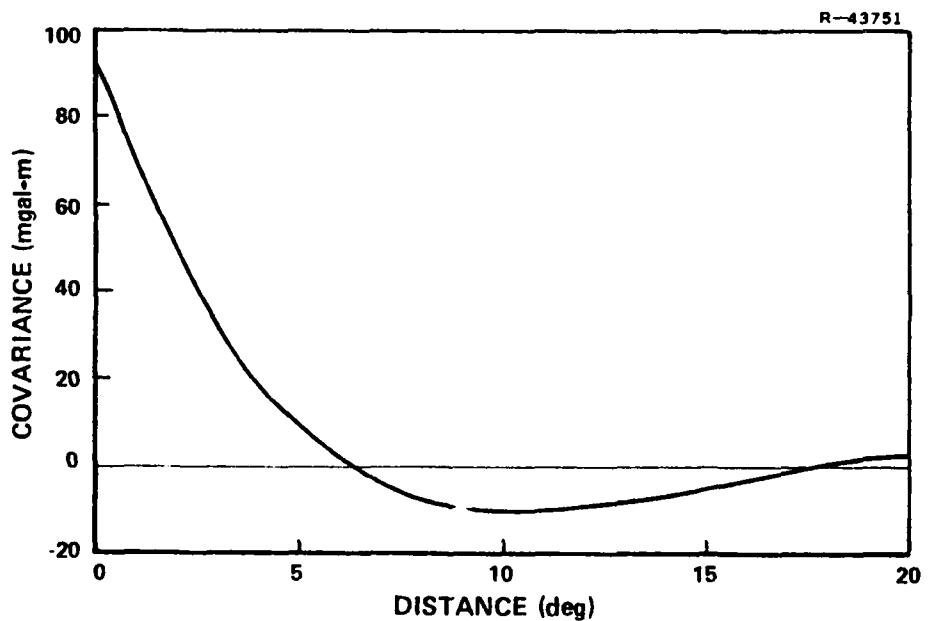
(b)   Residual Mean Gravity Anomaly/Geoid
       Height Cross-Covariance

Figure 3.1-4   Model Covariances

in Table 3.1-1. The mean discrepancy is less than 1 mgal and the standard deviation about 4 mgal. The distribution of the differences closely approximates a normal distribution. It should be emphasized that the observed differences include four separate effects:

- Errors in GEOS-3 geoid height measurements

- Incorrect statistical modeling

- Errors due to finite data extent and discretization

- Errors in surface gravity survey data

Any errors introduced by approximations in the GEOFAST algorithm itself are too small to be seen in this comparison (See Ref. 21).

TABLE 3.1-1

STATISTICS OF THE DIFFERENCE BETWEEN GEOFAST MEAN
GRAVITY ANOMALY ESTIMATES AND SURFACE REFERENCE DATA

REGION (Fig. 3.1-2)		MEAN (mgal)	STANDARD DEVIATION (mgal)	MAXIMUM MAGNITUDE (mgal)
10° x 10°		0.6	4.1	11.7
5° x 5°	A	1.3	2.8	6.7
	B	-3.1	3.1	-8.5
	C	3.8	3.9	8.2
	D	0.4	3.1	11.7

Comparisons were also made at DMAAC with estimates from the other two methods in use. Table 3.1-2 summarizes

TABLE 3.1-2

COMPARISONS BETWEEN ALGORITHMS

RMS DIFFERENCE (mgal)	GEOFAST	SPACE COLLOCATION	INVERSE STOKES	SURFACE DATA
GEOFAST	-	1.8	3.6	4.2
SPACE COLLOCATION		-	3.1	3.5
INVERSE STOKES			-	3.5

these results, including a comparison between each algorithm
and surface data. Space Collocation and Inverse Stokes both
agreed slightly better with the surface reference than GEOFAST
(3.5 versus 4.2 mgal), but differed from each other by almost
the same amount (3.1 mgal). GEOFAST differed from Space Col-
location by less than 2 mgal. Although these two methods are
based on the same assumptions, there was one known discrepancy
in this test case. The GEOFAST covariance construction ignored
the fact that the E-W distance between grid points decreases
with increasing latitude, instead using an average distance
valid at 27 deg N latitude. This introduces an error of 5-10%
which could account for up to 1 mgal rms difference. This
source of error was avoided on the second test case by using a
different construction (Section 3.2).

        Overall, the results verified the accuracy of the
GEOFAST estimates and the suitability of the method for possi-
ble use with GEOS-3 geoid height data. The relatively small
size of this first test case (N=225) did not admit meaningful
timing and efficiency comparisons to be made.

3.2 TEST CASE NO. 2

The objective of this test case was to demonstrate
the ability of GEOFAST to process high density along-track
data. Accordingly, the database for the second test case was
the GEOS-3 adjusted along-track point geoid height library
(Ref. 3). This data has been smoothed along-track to a 1 sec
(7 km) spacing, and adjusted to minimize track crossing dis-
agreement. Data contained in the same 20 deg by 20 deg square
used in Test Case No. 1 were obtained from DMAAC and amounted
to about 90,000 points. This was the base data from which the
1 deg grid values were obtained for the previous case. Resid-
ual geoid heights were obtained as before by subtracting a
spherical harmonic expansion to degree and order 12. This
reference geoid was computed on a 30 min grid and all data
points within a single grid square were compensated identi-
cally.

A transformation of coordinates was made in order to
obtain gridded data for the GEOFAST algorithm in which the
distance between points is constant in both directions. A
Lambert projection (Ref. 7) was used to map a spherical cap of
15 deg radius centered on the test area, onto a circular disc
in the plane. The spherical coordinates of latitude (ϕ) and
longitude (λ) were thereby mapped into cartesian coordinates
(x,y) in such a way that distance distortion was minimized.
The equations of this transformation are

$$
\begin{bmatrix} \tilde{x} \\ \tilde{y} \\ \tilde{z} \end{bmatrix}
=
\begin{bmatrix} \sin \phi_0 & 0 & -\cos \phi_0 \\ 0 & 1 & 0 \\ \cos \phi_0 & 0 & \sin \phi_0 \end{bmatrix}
\begin{bmatrix} \cos \lambda_0 & \sin \lambda_0 & 0 \\ -\sin \lambda_0 & \cos \lambda_0 & 0 \\ 0 & 0 & 1 \end{bmatrix}
\begin{bmatrix} \cos \phi \cos \lambda \\ \cos \phi \sin \lambda \\ \sin \phi \end{bmatrix}
$$

$$(3.2-1)$$

35

$$x = \rho\tilde{y} \quad , \quad y = -\rho\tilde{x} \quad , \quad \rho = \frac{180}{\pi} \sqrt{\frac{2}{1+\tilde{z}}} \qquad (3.2\text{-}2)$$

where $\phi_0 = 27$ deg and $\lambda_0 = 295$ deg, and result in less than
0.5% distance distortion for a 15 deg cap. The mapping is
displayed graphically in Fig. 3.2-1, where x and y are meas-
ured east and north, in degrees of great circle distance, from
the origin at 27 deg N latitude and 295 deg E longitude. The
data were then further restricted to a 15 deg by 15 deg square
in the plane whose exact location was determined by the avail-
ability of surface reference data. Figure 3.2-2 shows the
reduced region with the origin shifted to coincide with x=-8,
y=-6 in Fig. 3.2-1. The mean residual geoid height over this
region was subtracted from the data to remove bias.

The second test case was split into two subcases for
purposes of timing and accuracy comparisons. These were

- Case 2A: 1 deg by 1 deg grid (N=225)
- Case 2B: 30 min by 30 min grid (N=900)

where N represents the total number of grid points in the 15
deg square. The gridded geoid heights were obtained by simple
averaging with respect to x,y coordinates.

The gridded data thus obtained was processed by GEOFAST
(in a single computation) to produce residual mean gravity
anomalies at the same grid points as the residual geoid heights.
The model covariance functions were the same as those used in
the first test case (Fig. 3.1-4). For surface reference data
the 5 min gravity library anomalies were reduced by the spher-
ical harmonic model to degree and order twelve, and then mapped
onto a plane and gridded in exactly the same manner as the
GEOS-3 data. Although in practice the mean gravity anomaly

36
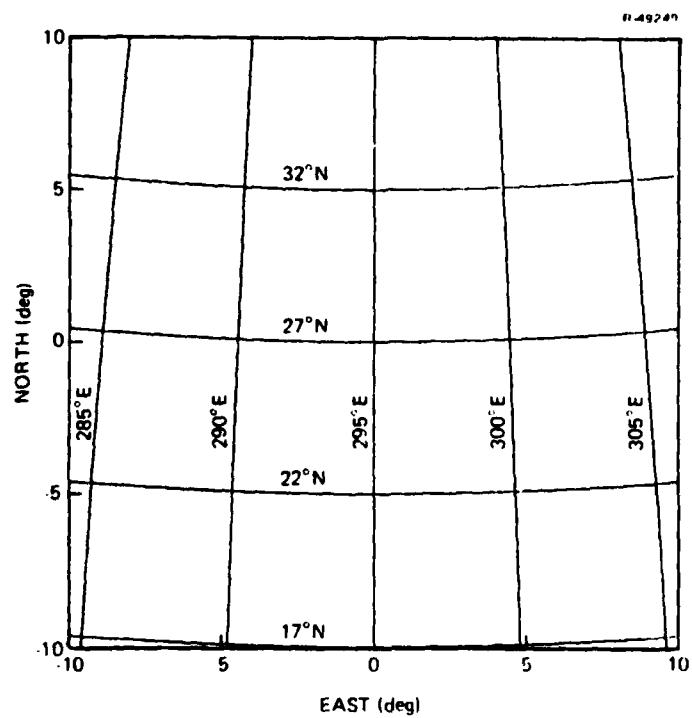
Figure 3.2-1   Lambert Transformation
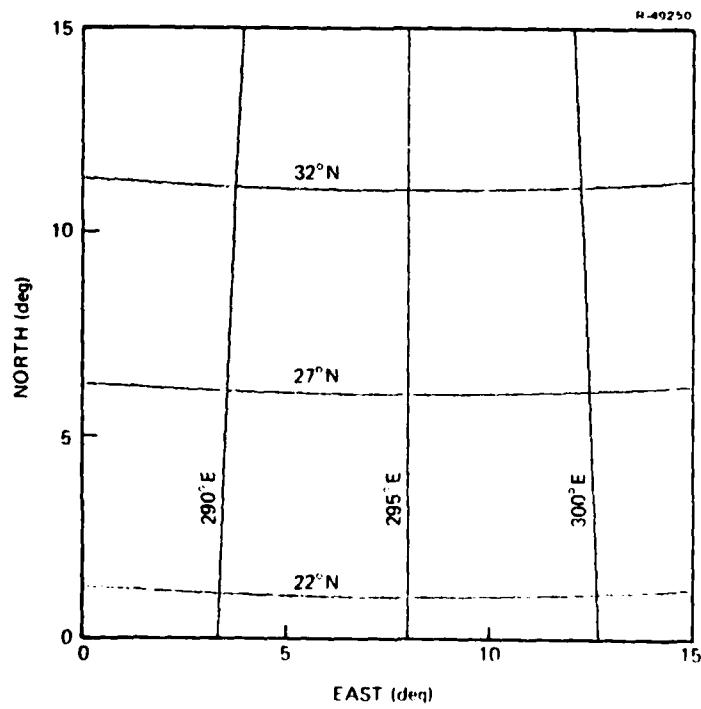
Figure 3.2-2   Reduced Estimation Region

estimtates would be mapped back to latitude and longitude co-
ordinates, this was not required for the present purposes.

The residual GEOS-3 geoid heights for both grid spac-
ings (1 deg and 30 min) are shown in Fig. 3.2-3, and the GEOFAST
residual mean gravity anomaly estimates are shown in Fig. 3.2-4.
The increased resolution at the higher density is apparent,
particularly in the region near Bermuda and in the Bahamas.
The estimates were differenced with the surface reference re-
sidual anomalies and the statistics of this comparison are
given in Tables 3.2-1 and 3.2-2. Three concentric square re-
gions were considered: the central 5 deg square, the central
10 deg square, and the 15 deg square. As expected the accuracy
of the estimates decreased toward the edge of the finite data
base. The mean difference in all cases was less than 1 mgal.

The difference standard deviation of 3.2 mgal for the
5 deg region with the 1 deg grid agreed closely with the result
from Test Case No. 1. This increased to only 4.1 mgal with the
30 min grid, whereas theory predicts a $\sqrt{N}$ dependence for a fac-
tor of two increase. Over the 15 deg region the values were
7.5 mgal and 10.7 mgal, respectively, which is an increase of
about 40%. Maximum differences were dominated by the presence
of Bermuda which is not adequately modeled in the covariance
structure. Even so, this singularity is estimated with much
sharper definition at the higher density grid. Also noteworthy
is the good accuracy obtained with gridding by simple averaging,
although this property depends on the smoothness of the data.
The geographical distribution of the differences between sur-
face data and GEOFAST estimates was also analyzed. Some of
the difference, although clearly not all, at the lower and
upper boundaries in Case 2B appears to be due to GEOFAST edge
error (See Ref. 21).
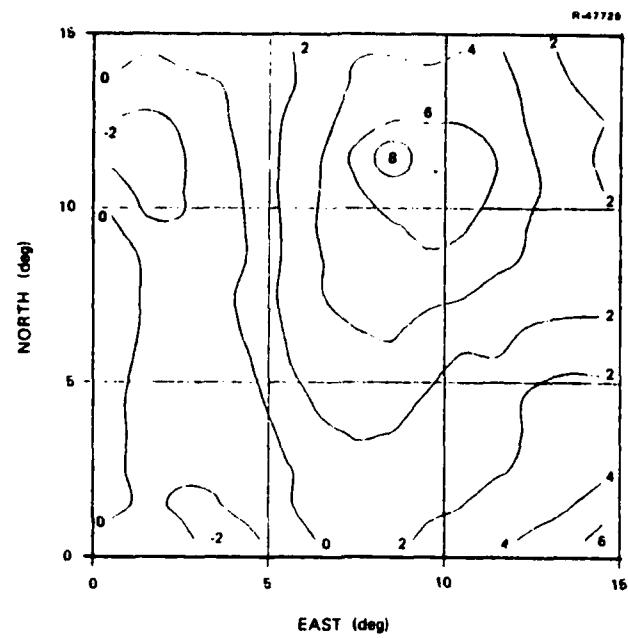
(a) Case 2A (1 deg grid)
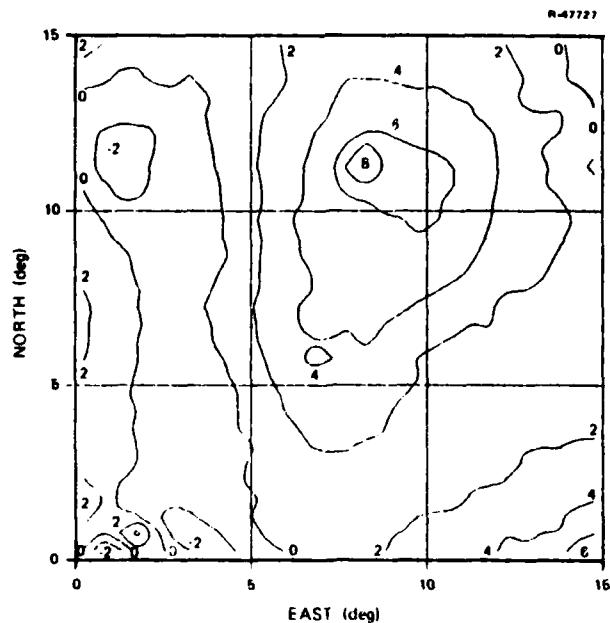
(b) Case 2B (30 min grid)

Figure 3.2-3   Residual GEOS-3 Geoid Heights
                 for Test Case No. 2 (m)
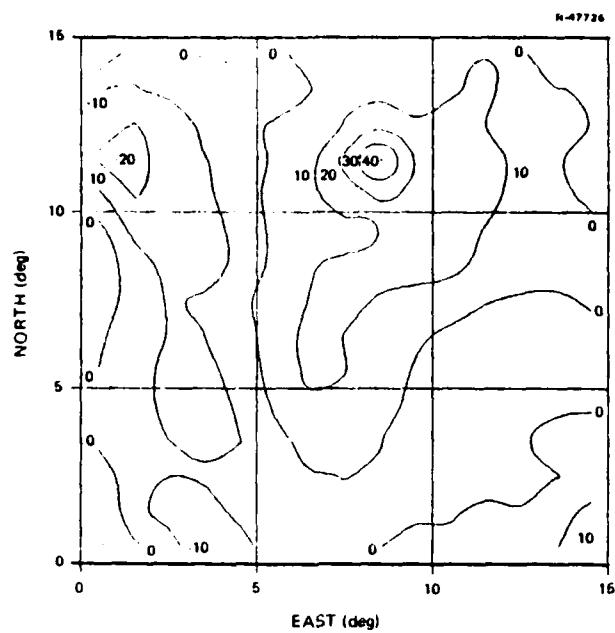
(a) Case 2A (1 deg grid)
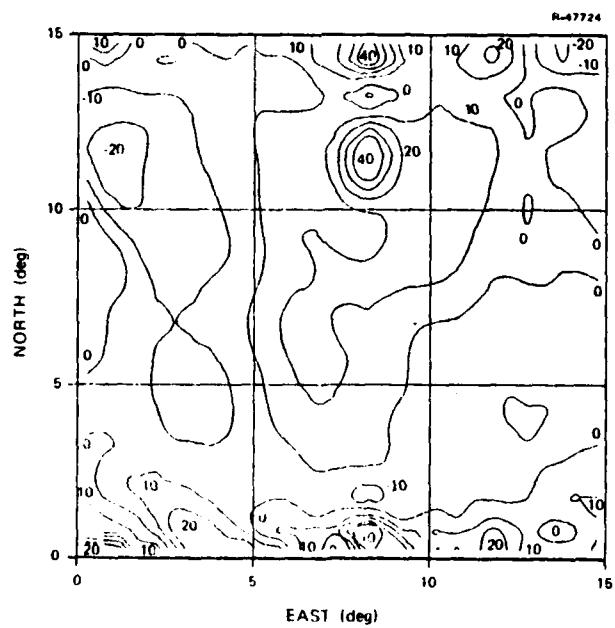
(b) Case 2B (30 min grid)

Figure 3.2-4   GEOFAST Residual Mean Gravity Anomaly
                  Estimates for Test Case No. 2 (mgal)

TABLE 3.2-1

DIFFERENCES BETWEEN GEOFAST MEAN GRAVITY ANOMALY ESTIMATES
AND SURFACE REFERENCE DATA FOR CASE 2A (1 deg GRID)

REGION (CENTERED)	MEAN (mgal)	STANDARD DEVIATION (mgal)	MAXIMUM MAGNITUDE (mgal)
5°×5°	-0.3	3.2	6.3
10°×10°	0.2	5.0	28.6[*]
15°×15°	0.8	7.5	28.6[*]

[*]Maximum occurs at the Bermuda rise.

TABLE 3.2-2

DIFFERENCES BETWEEN GEOFAST MEAN GRAVITY ANOMALY ESTIMATES
AND SURFACE REFERENCE DATA FOR CASE 2B (30 min GRID)

REGION (CENTERED)	MEAN (mgal)	STANDARD DEVIATION (mgal)	MAXIMUM MAGNITUDE (mgal)
5°×5°	-0.4	4.1	15.6
10°×10°	0.1	8.8	136.[*]
15°×15°	0.7	10.7	136.[*]

[*]Maximum occurs at the Bermuda rise.

With two different grids, computer time comparisons can be made (Table 3.2-3). As indicated, the computer time used in pre-processing to obtain gridded data was modest and nearly the same for both grids. The total time used by the GEOFAST algorithm increased by a factor of about six when the number of grid points increased by a factor of four. The analysis in Section 2 predicts an asymptotic $N\log_2 N$ dependence which would

TABLE 3.2-3

GEOFAST ALGORITHM COMPUTATIONAL EFFICIENCY

STAGE	TIME ON IBM 370 (min)	
	CASE 2A (N=225)	CASE 2B (N=900)
PRE-PROCESSING	<2	<2
TRANSFORM COVARIANCES	~1	~5
COMPUTE ESTIMATES	~1	~7
TOTAL GEOFAST	~2	~12

result in a ratio of about five. Considering the relatively small size of N this is acceptable agreement. The required time to compute 900 estimates was 12 min on an IBM 370/3033 computer, and would correspond to less than 2 min on a CDC 7600.[*] The results of this test justify the conclusion that the GEOFAST algorithm has the ability to process high density data with modest pre-processing, and to produce high resolution estimates of good quality with considerable efficiency.

---

*Estimated time on a CDC 7600 computer is based on benchmark testing conducted by the author.

4.   SUMMARY

        An algorithm has been presented which allows the
rapid calculation of minimum-variance estimates from high-
density gravity data. The GEOFAST method uses frequency do-
main techniques to achieve a complexity of order $N\log_2 N$ where
N is the number of data points. This efficiency is obtained
by exploiting two structures commonly found in gravimetric
applications:

● Input data that is regularly spaced on a
cartesian grid (after pre-processing)

● Statistical covariance models that are
stationary (or shift-invariant).

The resulting algorithm has been implemented in two-dimensions
and is well suited to the processing of very large gravity
data bases. A balance between accuracy and computer time may
be controlled by the choice of design parameters.

        The GEOFAST algorithm has been used to estimate mean
gravity anomalies from about 90,000 GEOS-3 geoid height values
suitably gridded to 900 points on a 15 deg square at a 30 min
resolution (Fig. 4-1). Agreement with surface gravity data
was relatively good and computer running time verified the
theoretical bounds. It is possible to extend the algorithm
further so that the two basic assumptions need hold only approx-
imately, thus considerably enhancing the range of application.
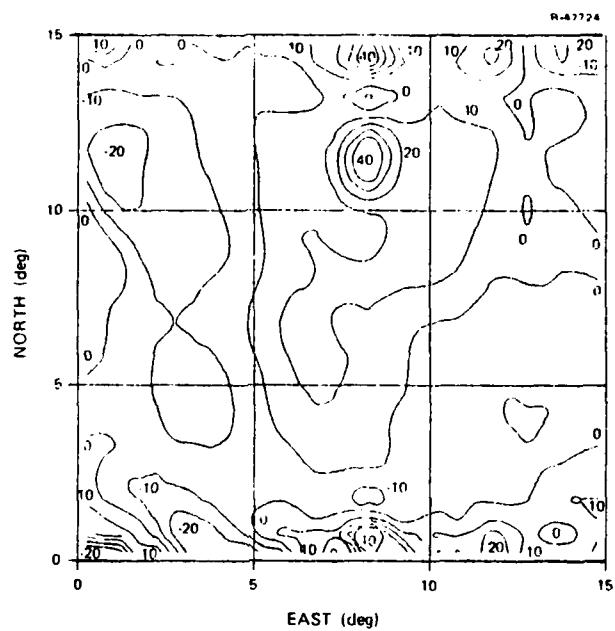
Figure 4-1   GEOFAST Residual Mean Gravity Anomaly
               Estimates at 30 min Resolution (mgal)

APPENDIX A
GEOFAST: ONE-DIMENSIONAL THEORY

This appendix presents a brief development of the mathematical theory underlying the one-dimensional GEOFAST algorithm. The material is condensed from Ref. 10, where further details may be found, and is included here for completeness. Some familiarity with these results is required for an understanding of the two-dimensional theory discussed in Appendix B.

A.1 TOEPLITZ AND CIRCULANT MATRICES

Toeplitz matrices are a class of n×n, real-valued matrices which includes the covariance matrices from stationary random processes. More formally, a matrix T is of the Toeplitz type if there is a real-valued function, t_ℓ, such that the elements of T obey

$$[T]_{jk} = t_{k-j} \quad , \qquad 0 \leq j, \; k \leq n-1 \qquad (A.1-1)$$

A Toeplitz matrix is defined by its first row and column since $[T]_{j+1,k+1} = [T]_{jk}$. If T is an autocovariance or a cross-covariance matrix, then t_ℓ is the corresponding covariance function. The matrix T is symmetric if the function t_ℓ is even.

Circulant matrices are a subset of Toeplitz matrices with an especially simple form under Fourier transformation. A Toeplitz matrix is a circulant if the function t_ℓ obeys

$$t_{-\ell} = t_{n-\ell} \quad , \quad \ell = 1, \ldots, n-1 \qquad (A.1-2)$$

A circulant matrix is defined by its first row since each row is equal to the row preceding it shifted one element to the right, with the last element "wrapped around" to the first place. For example, a circulant matrix with the first row $(c_0, c_1, \ldots, c_{n-1})$ necessarily has its second row given by $(c_{n-1}, c_0, c_1, \ldots, c_{n-2})$. While circulant matrices themselves do not appear frequently, their properties are useful in dealing with the more general Toeplitz matrices.

Circulant matrices have the special property that they are diagonalized by the Discrete Fourier Transformation (DFT). The n-point DFT matrix F is the n×n, symmetric, unitary, complex-valued matrix whose elements are[*]

$$[F]_{jk} = \frac{1}{\sqrt{n}} \exp\left[-\frac{2\pi i j k}{n}\right] , \quad 0 \le j, k \le n-1 \qquad (A.1-3)$$

and its inverse is easily seen to be $F^\dagger$. The DFT of an n-vector of complex numbers, $\underline{x}$, is defined by the relations (Ref. 9)

$$\underline{x}' = F\,\underline{x}, \quad \underline{x} = F^\dagger\,\underline{x}' \qquad (A.1-4)$$

The matrix similarity transformation corresponding to Eq. A.1-4 is given by

$$C' = F\,C\,F^\dagger \qquad (A.1-5)$$

where C is an n×n matrix of complex numbers and C' is its representation in the Fourier transform domain. The usefulness of the circulant matrix definition depends largely on the following result.

---

[*]The symbol i denotes $\sqrt{-1}$, and the superscript (†) denotes the complex conjugate transpose.

The Fourier transformation, Eq. A.1-5, of any circulant matrix C is the diagonal matrix

$$C' = \mathrm{diag}(c'_0, \ldots, c'_{n-1}) \qquad\qquad \text{(A.1-6)}$$

where $\underline{c}'$ is the discrete power spectrum

$$\underline{c}' = \sqrt{n}\, F^{\dagger}\, \underline{c} \qquad\qquad\qquad \text{(A.1-7)}$$

and $\underline{c}$ corresponds to the first row of C. Moreover, any diagonal matrix is the Fourier transform of a circulant matrix, defined by Eqs. A.1-6 and A.1-7. If the matrix C is symmetric the inverse transform $F^{\dagger}$ may be replaced by F in Eq. A.1-7. A proof of this result may be found in Refs. 2 and 4. This theorem is also equivalent to the well known relationship between discrete convolutions and discrete Fourier transforms proved in Ref. 20.

Since circulant matrices are diagonalized by the DFT they can be multiplied or inverted in order $n\log_2 n$ operations. Specifically, if

$$\underline{y} = C\, \underline{x} \qquad\qquad\qquad\qquad \text{(A.1-8)}$$

then

$$\underline{y}' = C'\, \underline{x}' = \mathrm{diag}(\underline{c}')\, \underline{x}' \qquad\qquad \text{(A.1-9)}$$

where $\underline{x}'$ and $\underline{y}'$ are defined as in Eq. A.1-4 and $\underline{c}'$ in Eq. A.1-7. It follows that

$$y'_j = c'_j \cdot x'_j \quad , \quad x'_j = y'_j / c'_j \qquad\qquad \text{(A.1-10)}$$

so that either $\underline{y}$ or $\underline{x}$ can be found with two FFT's, n scalar multiplications, and one inverse FFT. The matrix multiplication

47

in Eq. A.1-8 is also equivalent to the circular convolution

$$y_j = \sum_{k=o}^{n-1} c_{k-j} \, x_j \qquad\qquad \text{(A.1-11)}$$

so that fast multiplication is the same as fast convolution.

A.2   THE TRANSFORM OF A WINDOWED TOEPLITZ MATRIX

This section describes the calculation of the Fourier transform of a "windowed" Toeplitz matrix.   An algorithm to accomplish this for a single superdiagonal band in approximately nlogn computer operations is derived here from the result of Section A.1.   A windowed Toeplitz matrix is one which has been multiplied by a diagonal matrix, W, to form

$$U = W \, T \, W \qquad\qquad \text{(A.2-1)}$$

The matrix W is defined by a window function, w_ℓ, such that

$$W = \text{diag}(w_0, \ w_1, \ \ldots, \ w_{n-1}) \qquad\qquad \text{(A.2-2)}$$

The window function is related to the way in which data is processed, and is described in the next section.   For a general discussion of window functions in frequency domain data processing, see Refs. 8 and 19.   Note that one choice for W is simply $W = I$ where I is the n×n identity matrix.   Thus, the class of windowed Toeplitz matrices includes all Toeplitz matrices.

The DFT of the windowed Toeplitz matrix in Eq. A.2-1 is

$$T' = F W T W F^{\dagger} \qquad \text{(A.2-3)}$$

The work of deriving a useful element-by-element expression for this matrix is divided into two parts: first, obtaining an expression for T' in terms of transforms of diagonal and circulant matrices and, second, applying the circulant theorem of Section A.1 to deduce an efficient computational formula.

The matrix T is extended to a $2n \times 2n$ circulant matrix $\tilde{T}$ by the definitions

$$[\tilde{T}]_{jk} = c_{k-j} \quad , \qquad 0 \le j, \ k \le 2n-1 \qquad \text{(A.2-4)}$$

where

$$c_{\ell} = \begin{cases} t_{\ell} & 0 \le \ell \le n-1 \\ 0 & \ell = n \\ t_{\ell-2n} & n+1 \le \ell \le 2n-1 \end{cases} \qquad \text{(A.2-5)}$$

and $c_{-\ell} = c_{2n-\ell}$ for $1 \le \ell \le 2n-1$. The matrix $\tilde{T}$ has the partitioned form

$$\tilde{T} = \begin{bmatrix} T & R \\ R & T \end{bmatrix} \qquad \text{(A.2-6)}$$

where R is a Toeplitz matrix corresponding to the function

$$r_{\ell} = \begin{cases} t_{\ell-n} & \ell > 0 \\ \frac{1}{2}(t_{n-1} + t_{-n+1}) & \ell = 0 \\ t_{\ell+n} & \ell < 0 \end{cases} \qquad \text{(A.2-7)}$$

Also a $2n \times 2n$ extended version of W is defined by

$$\tilde{W} = \begin{bmatrix} W & 0 \\ 0 & 0 \end{bmatrix} \qquad (A.2\text{-}8)$$

The windowed Toeplitz matrix WTW may now be expressed in terms of the diagonal matrix $\tilde{W}$ and the circulant matrix $\tilde{T}$ by

$$\begin{bmatrix} WTW & 0 \\ 0 & 0 \end{bmatrix} = \tilde{W} \, \tilde{T} \, \tilde{W} \qquad (A.2\text{-}9)$$

Introducing the n×2n sampling matrix S defined by

$$S = \begin{bmatrix} 1 & 0 & . & . & . & 0 \\ 0 & 0 & 1 & . & . & 0 \\ & & & & & . \\ & & & & & . \\ & & & & & . \\ . & . & . & 0 & 1 & 0 \end{bmatrix} \qquad (A.2\text{-}10)$$

it may be verified that

$$T' = S \, \tilde{F} \, \tilde{W} \, \tilde{T} \, \tilde{W} \, \tilde{F}^{\dagger} S^{T} \qquad (A.2\text{-}11)$$

where $\tilde{F}$ is the 2n×2n Discrete Fourier Transformation defined by Eq. A.1-3 with n replaced by 2n. Equation A.2-11 expresses T' as the result of sampling every other row and column of a matrix which is the transform of a product of diagonal window matrices and a circulant matrix.

The application of the circulant properties stated in Section A.1 produces the desired expression for T'. Equation A.2-11 may be written as

$$T' = S \, \tilde{W}'\tilde{T}'\tilde{W}' S^{T} \qquad (A.2\text{-}12)$$

where $\tilde{W}'$ and $\tilde{T}'$ are the transformed matrices

$$\tilde{W}' = \tilde{F} \; \tilde{W} \; \tilde{F}^{\dagger} \qquad\qquad \text{(A.2-13)}$$

$$\tilde{T}' = \tilde{F} \; \tilde{T} \; \tilde{F}^{\dagger} \qquad\qquad \text{(A.2-14)}$$

Using Eqs. A.1-5 and A.1-7 with F replaced by $F^{\dagger}$ shows that the first of these matrices is a circulant, with the elements

$$[\tilde{W}']_{jk} = \Omega_{k-j}, \; 0 \le j, \; k \le 2n-1 \qquad\qquad \text{(A.2-15)}$$

where Ω_{ℓ} is given by the transform

$$\Omega_0, \; \Omega_1, \; \ldots, \; \Omega_{2n-1}{}^{T} = \underline{\Omega} = \frac{1}{\sqrt{2n}} \; \tilde{F}^{\dagger} \begin{bmatrix} \underline{w} \\ \underline{0} \end{bmatrix} \qquad\qquad \text{(A.2-16)}$$

and $\underline{w}$ is the n-vector defined by the window function

$$\underline{w} = (w_0, \; w_1, \; \ldots, \; w_{n-1})^{T} \qquad\qquad \text{(A.2-17)}$$

It also follows directly from Eqs. A.1-5 and A.1-7 that the matrix $\tilde{T}'$ of Eq. A.2-14 is diagonal, of the form

$$\tilde{T}' = \text{diag} \; (\tau_0, \; \tau_1, \; \ldots, \; \tau_{2n-1}) \qquad\qquad \text{(A.2-18)}$$

where $\underline{\tau} = (\tau_0, \; \tau_1, \; \ldots, \; \tau_{2n-1})^{T}$ is defined by the vector $\underline{c}$ of Eq. A.2-5 via

$$\underline{\tau} = \sqrt{2n} \; \tilde{F} \; \underline{c} \qquad\qquad \text{(A.2-19)}$$

A useful element-by-element formula for T' is a consequence of Eq. A.2-12. Substitution of the definitions from

Eqs. A.2-10, A.2-15, and A.2-18, with some simplification, produces the expression[*]

$$[T']_{jk} = \sum_{\ell=0}^{2n-1} \Omega_{\ell-2j} \, \bar{\Omega}_{\ell-2k} \, \tau_\ell \qquad (A.2-20)$$

where Ω_ℓ is the transform of the window function (Eq. A.2-16) and τ_ℓ is the power spectrum of $\tilde{T}$ (Eq. A.2-19). The subscripts in Eq. A.2-20 are interpreted modulo 2n. In particular the elements of the mth superdiagonal band of T' can be written (for $0 \leq j \leq n-m-1$)

$$[T']_{j,j+m} = \sum_{\ell=0}^{2n-1} \rho_{\ell-2j}(m) \, \tau_\ell \qquad (A.2-21)$$

where

$$\rho_k(m) = \Omega_k \, \bar{\Omega}_{k-2m} \qquad (A.2-22)$$

Now Eq. A.2-21 can be recognized as a convolution, or alternatively as the product of a circulant matrix and a vector (Section A.1). As a result the band elements defined by Eq. A.2-21 can be computed in order $n\log_2 n$ operations.


A.3 WINDOWS AND BANDING

The impact of the window function on the structure of T' can be seen from Eqs. A.2-21 and A.2-22. The elements of the mth diagonal band are obtained by convolving the power

---

[*]The symbol $\bar{\Omega}_\ell$ represents the complex conjugate of the quantity Ω_ℓ. Since $\tilde{W}'$ is hermitian, $\Omega_{k-j} = \bar{\Omega}_{j-k}$.

52

spectrum τ_ℓ with the weighting function $\rho_\ell(m)$, which consists of the transformed data window multiplied by its conjugate shifted 2m elements to the right.

Two typical window functions and their transforms are shown in Fig. A.3-1. These windows are special cases of the Kaiser window function which has proved very useful in signal processing applications, and is defined in Refs. 15 and 19. Transforms of data windows are characterized by a mainlobe and a series of sidelobes of considerably reduced levels. As can be seen from the figure, the disparity between mainlobe and sidelobe levels becomes more pronounced as the width of the mainlobe is increased. This behavior is reflected in the numerical structure of the matrix T'. The elements of T' corresponding to the shaded area of Fig. A.3-2 cannot be neglected because the mainlobes of Ω_ℓ and $\Omega_{\ell-2m}$ overlap for these elements. However, the elements of T' outside the shaded area of the figure are the product of the sidelobes of Ω_ℓ together with the power spectrum τ_ℓ. When the sidelobes are made sufficiently small, these elements may be neglected. The key idea in the band-diagonal algorithm is the control of out-of-band covariance elements by choice of a data window with sufficiently small sidelobes.

A final transformation must be applied to form the frequency domain covariance matrix into a band-diagonal structure. Because it is known that the data must always be real-valued, the sine-cosine transform coefficients are sufficient to describe the data, rather than the full, complex set of Fourier coefficients. The practical importance of this last transformation is the elimination of the elements in the upper right and lower left corners of T' as shown in Fig. A.3-2.

R-29067

FREQUENCY DOMAIN   SPACE DOMAIN

RECTANGULAR WINDOW: MAINLOBE WIDTH = 1

R-29069

FREQUENCY DOMAIN   SPACE DOMAIN

KAISER WINDOW: MAINLOBE WIDTH = 2
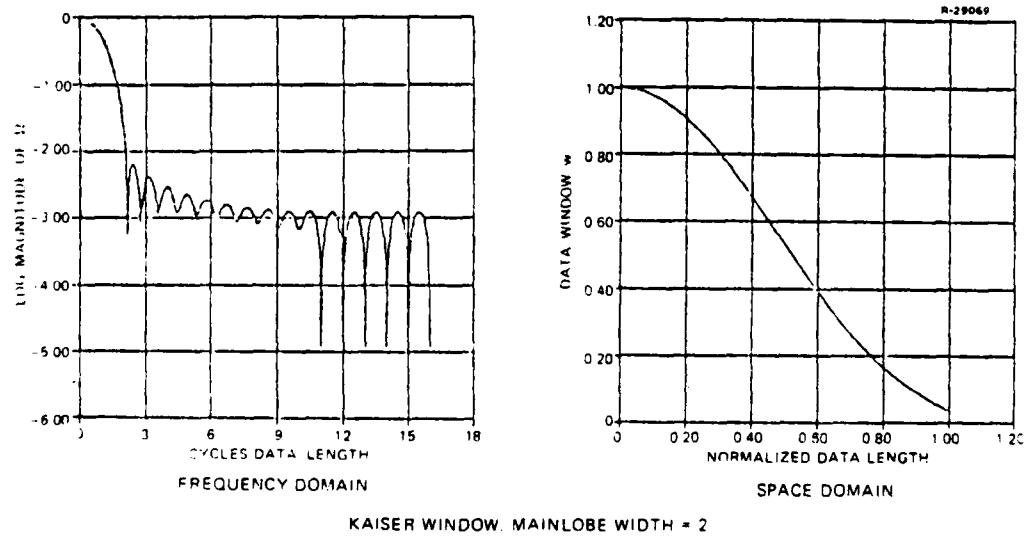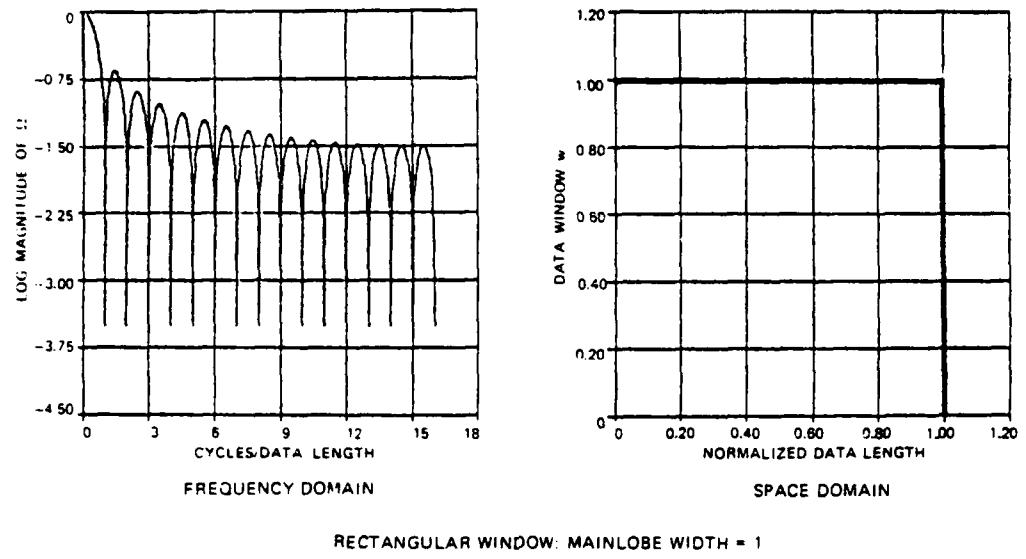
Figure A.3-1   Data Windows and Transforms
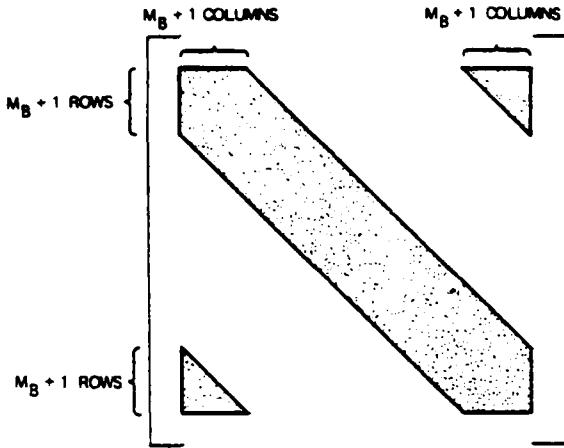
Figure A.3-2   Structure of Covariance Matrix
                 Under Fourier Transformation

The transformation to sine-cosine coefficients corresponds to modifying the complex transformation of Eq. A.2-3 to the real form

$$T' = H\ F\ W\ T\ W\ F^\dagger H^\dagger \qquad\qquad (A.3\text{-}1)$$

where H is an n×n complex transformation from exponential Fourier coefficients to sine-cosine coefficients. The elements of H are defined by

$$(A.3\text{-}2)$$

The first n/2+1 rows of H generate the cosine coefficients of
the data, while the last n/2-1 rows generate the sine coefficients.

The result of using the modified transformation (Eq.
A.3-1) in the definition of T' is shown in Fig. A.3-3. The
matrix T' may now be approximated by the real band-diagonal
matrix, D', neglecting the small elements due to the sidelobes
of Ω_ℓ. In addition the elements of D' may be partitioned into
blocks of dimension n/2+1 and n/2-1 so that the dimension of
the largest system of equations to be solved is approximately
halved.
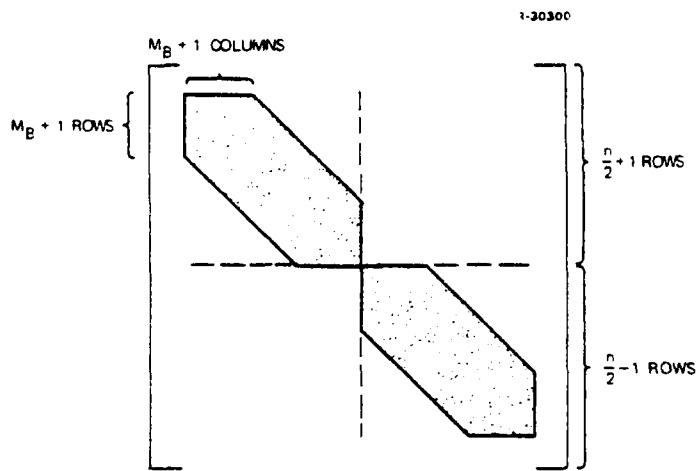
Figure A.3-3   Structure of Covariance Matrix Under
                  Sine-Cosine Transformation

A.4 APPROXIMATE SOLUTION OF TOEPLITZ EQUATIONS

The solution of the linear system

$$\underline{y} = T \, \underline{x}$$

(A.4-1)

56

can be obtained efficiently using the transformation of Eq.
A.3-1 when T is a symmetric Toeplitz matrix. If A = HFW and

$$\underline{y}' = A \, y \quad , \quad \underline{x} = A^\dagger \underline{x}' \qquad \text{(A.4-2)}$$

then

$$\underline{y}' = T'\underline{x}' \quad , \quad T' = A \, T \, A^\dagger \qquad \text{(A.4-3)}$$

where T' is symmetric and has the structure in Fig. A.3-3.
This is a generalization of the circulant case where T' is
diagonal. An efficient aproximate solution to Eq. A.4-3 is
found by replacing the exact matrix T' by its banded approxi-
mation D'. The special structure of D' is exploited by employ-
ing the band-diagonal implementation of the Cholesky decompo-
sition algorithm (Ref. 6, Section 2.3) for the solution of
linear equations. The number of numerical operations required
is of order $(m_B+1)^2 n$ for large n, where m_B is the number of
superdiagonal bands.

The magnitude of the band approximation error can be
expressed by the quantity

$$\varepsilon = \left[\frac{E(\delta\underline{x} \; \delta\underline{x})}{E(\underline{x}^T\underline{x})} \right]^{1/2} \qquad \text{(A.4-4)}$$

which is the relative rms error in the solution $\underline{x}$ to Eq. A.4-1
due to replacing T' by D' in Eq. A.4-3. The error in the
solution due to the neglected out-of-band elements in T' is
controlled by adjusting the matrix bandwidth m_B through the
choice of the data window function defined in Section A.3.
Bounds on the computational error arising from this source
were computed in Ref. 10 and show that $m_B \leq 10$ is sufficient
for most applications.

There is, however, a penalty for the use of highly tapered data windows (large m_B). It can be shown that the condition number K of the matrix T' satisfies (Ref. 6)

$$K(T') = \lambda_{max}(T')/\lambda_{min}(T') \geq w_o^{-2} \qquad (A.4\text{-}5)$$

where w_o is the smallest window coefficient and $\lambda(T')$ denotes an eigenvalue of the matrix T'. When K is large the matrix is ill-conditioned and computing its inverse by the Cholesky method may fail due to the appearance of negative diagonal elements. To compensate for ill-conditioning the equations A.4-3 are modified by adding a small constant δ to the diagonal so that

$$T' = A\, T\, A^{\dagger} + \delta\, I \qquad (A.4\text{-}6)$$

The modified problem is well-conditioned since $\lambda_{min}(T') \geq \delta$ and $K \leq \lambda_{max}(T')/\delta$. By inverting the transformation (Eq. A.4-3) the modified equations are found to be

$$\underline{y} = (T + \delta\, W^{-2})\, \underline{x} \qquad (A.4\text{-}7)$$

where W is the diagonal window matrix.

When T is a covariance matrix Eq. A.4-7 may be interpreted as the addition of uncorrelated measurement noise to the model. In the modified problem the quality of the data is gradually de-emphasized as the ends of the data interval are approached, and points for which the signal-to-noise ratio

$$S_k = t_o w_k^2/\delta \qquad (A.4\text{-}8)$$

is less than one, may be regarded as having been lost. The percentage of data points for which S_k is less than one defines a performance index, called "data de-emphasis," which is

58

a function of δ and m_B. The results presented in Ref. 10 show
that a relative error of less than 1% may be achieved with a
data de-emphasis of less than 10% for typical applications.

APPENDIX B

GEOFAST: TWO-DIMENSIONAL THEORY

This appendix extends the mathematical theory under-
lying the GEOFAST algorithm to two dimensions. Since a basic
understanding of the one-dimensional theory (Ref. 10) is re-
quired, the necessary results are developed in Appendix A.
Thus the two appendices taken together are self-contained.

B.1   BLOCK CIRCULANT MATRICES AND KRONECKER PRODUCTS

The relationship between circulant matrices and the
Discrete Fourier Transform (DFT) is described in Appendix A.
The DFT matrix in one dimension is defined by[*]

$$[F]_{jk} = \frac{1}{\sqrt{n}} \omega^{jk} \quad , \quad \omega = \exp\left[-\frac{2\pi i}{n}\right] \qquad \text{(B.1-1)}$$

where ω is the complex n^{th} root of unity and n is the number
of points. A circulant matrix satisfies

$$[C]_{jk} = c_{k-j(\text{mod } n)} \quad 0 \le j,k \le n-1 \qquad \text{(B.1-2)}$$

and is defined by its first row "circulated". The significance
of these definitions is that any circulant matrix is diagonal-
ized by the DFT, that is,

$$C' = F C F^{\dagger} = \sqrt{n} \text{ diag } [F^{\dagger}\underline{c}] \qquad \text{(B.1-3)}$$

---

[*]The symbol i denotes $\sqrt{-1}$ and the superscript ($\dagger$) denotes the
  complex conjugate transpose.

60

is a diagonal matrix (Refs. 2 and 4). This relationship extends to two dimensions with the appropriate definitions as shown below.

B.1.1   The DFT as a Kronecker Product

The DFT in two dimensions is defined by

$$z'_{pq} = \frac{1}{\sqrt{n_1 n_2}} \sum_{j=o}^{n_1-1} \sum_{k=o}^{n_2-1} z_{jk} \, \omega_1^{pj} \, \omega_2^{qk} \qquad (B.1\text{-}4)$$

where z_{jk} is an $n_1 \times n_2$ data matrix and ω_1, ω_2 denote the complex roots of unity

$$\omega_1 = \exp\left[-\frac{2\pi i}{n_1}\right] \quad , \quad \omega_2 = \exp\left[-\frac{2\pi i}{n_2}\right] \qquad (B.1\text{-}5)$$

Analogous to the DFT matrix in Eq. B.1-1, the operator defined by Eq. B.1-4 is a tensor of fourth rank whose components are of the form a_{pqjk}.

It is more convenient to represent the DFT in matrix form by expressing z_{jk} (row-wise) as a vector $\underline{z}$, such that

$$\underline{z}' = F \, \underline{z} \qquad (B.1\text{-}6)$$

is equivalent to Eq. B.1-4. When this is done the $n_1 n_2 \times n_1 n_2$ matrix F is seen to assume a simple block structure, namely,

$$F = \begin{bmatrix} f_{1,11} \, F_2 & f_{1,12} \, F_2 & \cdots \\ f_{1,21} \, F_2 & f_{1,22} \, F_2 & \\ & & \end{bmatrix} \qquad (B.1\text{-}7)$$

61

where F_2 is the n_2-point DFT matrix defined by

$$[F_2]_{jk} = f_{2,jk} = \frac{1}{\sqrt{n_2}} \omega_2^{jk} \qquad (B.1-8)$$

and similarly for F_1. Each block in Eq. B.1-7 is of size $n_2 \times n_2$ and there are n_1 blocks in each row and column. This special structure is denoted by

$$F = F_1 \otimes F_2 \qquad (B.1-9)$$

and termed the Kronecker product of F_1 and F_2 (Ref. 2). Kronecker products define a special class of tensors with the important properties

$$(A \otimes B)(C \otimes D) = (AC \otimes BD)$$
$$(A \otimes B)^\dagger = (A^\dagger \otimes B^\dagger) \qquad (B.1-10)$$
$$(A \otimes B)^{-1} = (A^{-1} \otimes B^{-1})$$

where the matrices A, C and B, D are assumed to be conformably dimensioned.

For computational purposes it is convenient to evaluate the multiplication of a vector by a Kronecker product matrix in terms of ordinary matrix operations. The two product forms

$$\underline{y} = (A \otimes B)\ \underline{x}$$
$$Y = A\ X\ B^T \qquad (B.1-11)$$

are equivalent if $\underline{x}$, $\underline{y}$ are the row-by-row vector representations of the matrices X, Y. It is assumed that A is $n_1 \times n_1$, B is

62

$n_2 \times n_2$, and X, Y are $n_1 \times n_2$. This equivalence can be derived from the corresponding element-by-element formulas such as Eq. B.1-4.

B.1.2 Diagonalization of Block Circulant Matrices

By a block circulant matrix (with circulant blocks) is meant an $n_1 n_2 \times n_1 n_2$ matrix of the form

$$
C = \begin{bmatrix}
C_0 & C_1 & & C_{n_1-1} \\
\hline
C_{n_1-1} & C_0 & & C_{n_1-2} \\
\hline
 & & & \\
\hline
C_1 & C_2 & & C_0
\end{bmatrix}
\qquad \text{(B.1-12)}
$$

where each of the n_1 block matrices C_k is a circulant of dimension $n_2 \times n_2$. A special case of a block circulant matrix is the Kronecker product of two circulants C_1, C_2 of dimension n_1, n_2

$$
C = C_1 \otimes C_2 \qquad \text{(B.1-13)}
$$

In this case Eqs. B.1-3, B.1-9 and B.1-10 show that

$$
C' = F\, C\, F^\dagger = (F_1\, C_1\, F_1^\dagger) \otimes (F_2\, C_2\, F_2^\dagger) \qquad \text{(B.1-14)}
$$

is a diagonal matrix. The diagonal entries of C' are of the products of the diagonal entries of C_1', C_2'.

Of more interest is the fact that C' is diagonal for any block circulant C. This theorem is derived below. Let P_1 denote the primitive circulant matrix of dimension n_1

$$P_1 = \begin{bmatrix} 0 & 1 & 0 & . & . & 0 \\ 0 & 0 & 1 & . & . & 0 \\ . & & . & & & . \\ 0 & 0 & 0 & . & . & 1 \\ 1 & 0 & 0 & . & . & 0 \end{bmatrix} \qquad (B.1-15)$$

The matrix P_1 is orthogonal $(P_1 P_1^T = I)$ and generates a cyclic group of order n_1

$$\{P_1, \; P_1^2, \; \ldots \; , \; P_1^{n_1-1}, \; P_1^{n_1} = P_1^0 = I\} \qquad (B.1-16)$$

since the kth power of P_1 is a circulant whose first row is the kth unit vector. Furthermore any block circulant matrix may be represented as the sum

$$C = \sum_{k=o}^{n_1-1} (P_1^k \otimes C_k \qquad (B.1-17)$$

where each C_k is an $n_2 \times n_2$ circulant (see Eq. B.1-12). The theorem follows since

$$C' = F \; C \; F^\dagger = \sum_{k=o}^{n_1-1} (F_1 \; P_1^k \; F_1^\dagger) \otimes (F_2 \; C_k \; F_2^\dagger) \qquad (B.1-18)$$

and each factor in parentheses is the DFT of a circulant.

An explicit expression for the diagonal entries of C' can be obtained by reference to Eq. B.1-3. Since P_1^k is a circulant whose first row is the kth unit vector, $\underline{e}_k$, and C_k is a circulant with first row $\underline{c}_k$, it follows that

$$F_1 \; P_1^k \; F_1^\dagger = \mathrm{diag}[\sqrt{n}_1 \; F_1^\dagger \; \underline{e}_k]$$

$$F_1 \; C_k \; F_1^\dagger = \mathrm{diag}[\sqrt{n}_2 \; F_2^\dagger \; \underline{c}_k] \tag{B.1-19}$$

Eq. B.1-18 then becomes

$$C' = \mathrm{diag}[(\sqrt{n}_1 \; F_1 \otimes \sqrt{n}_2 \; F_2)^\dagger \; \underline{c}] \tag{B.1-20}$$

where $\underline{c}$ is the first row of C, or equivalently

$$\underline{c} = \sum_{k=o}^{n_1-1} \underline{e}_k \otimes \underline{c}_k \tag{B.1-21}$$

Note that these two-dimensional relations reduce to the one-dimensional forms if $n_2 = 1$, and also may be readily extended to higher dimensions in a natural way.

The converse theorem is also needed, namely that the DFT of a diagonal matrix D is a block circulant. Since any $n_1 n_2$-square diagonal matrix can be represented as

$$D = \sum_{k=o}^{n_1-1} [\mathrm{diag}(\underline{e}_k)] \otimes [\mathrm{diag} \; (\underline{d}_k)] \tag{B.1-22}$$

where $\underline{e}_k$ is a unit vector of dimension n_1 and $\underline{d}_k$ is a vector of dimension n_2,

$$C \equiv F^\dagger \; D \; F = \sum_{k=o}^{n_1-1} [F_1^\dagger \; \mathrm{diag}(\underline{e}_k) \; F_1] \otimes [F_2^\dagger \; \mathrm{diag}(\underline{d}_k) \; F_2] \tag{B.1-23}$$

The matrices in square brackets are circulants by virtue of the one-dimensional theory (Appendix A). But the Kronecker

product of two circulants is block circulant, and this prop-
erty is preserved under addition. Since C is a block circu-
lant Eq. B.1-20 can be inverted to obtain

$$\underline{c} = \left(\frac{1}{\sqrt{n_1}} F_1 \otimes \frac{1}{\sqrt{n_2}} F_2 \right) \underline{d} \qquad (B.1\text{-}24)$$

where $D = diag(\underline{d})$. In particular if $\underline{d} = \underline{d}_1 \otimes \underline{d}_2$ then
$C = C_1 \otimes C_2$ with the obvious definitions.

Since block circulants are diagonalized by the DFT
they can be multiplied or inverted in order $Nlog_2N$ operations
in complete analogy with the one-dimensional case (Appendix A).
If

$$\underline{y} = C \underline{x} \qquad (B.1\text{-}25)$$

then

$$\underline{y}' = diag(\underline{c}') \underline{x}' \qquad (B.1\text{-}26)$$

where prime denotes transform and $\underline{c}'$ is given by Eq. B.1-20.
Thus either $\underline{x}$ or $\underline{y}$ can be found with two FFT's, N scalar multi-
plications, and one inverse FFT.

The matrix multiplication in Eq. B.1-25 is also equiv-
alent to a two-dimensional circular convolution

$$y_{jk} = \sum_{p=o}^{n_1-1} \sum_{q=o}^{n_2-1} c_{p-j,q-k} \, x_{pq} \qquad (B.1\text{-}27)$$

where X, Y are the matrix forms of $\underline{x}$, $\underline{y}$, and the elements c_{jk}
form the vectors

66

$$\underline{c}_j^T = [c_{j0}, c_{j1}, \quad \cdots \quad , c_{j,n_2-1}] \tag{B.1-28}$$

which define the circulants C_j in Eqs. B.1-12. In the special case that $C = A \otimes B$, with A and B circulant, Eq. B.1-27 is simplified to

$$y_{jk} = \sum_{p=o}^{n_1-1} a_{p-j} \sum_{q=o}^{n_2-1} b_{q-k} \, x_{pq} \tag{B.1-29}$$

which is a sequence of row and column convolutions (see Eq. B.1-11).

B.2 THE TRANSFORM OF A WINDOWED BLOCK TOEPLITZ MATRIX

B.2.1 Matrix Representation of the Transform

A block Toeplitz matrix (with Toeplitz blocks) is an $n_1 n_2 \times n_1 n_2$ matrix of the form (see Eq. B.1-12)

$$T = \begin{bmatrix} T_0 & T_1 & & T_{n_1-1} \\ T_{-1} & T_0 & & T_{n_1-2} \\ & & & \\ T_{-(n_1-1)} & T_{-(n_1-2)} & & T_0 \end{bmatrix} \tag{B.2-1}$$

where each block T_k is a Toeplitz matrix of dimension $n_2 \times n_2$. Such matrices arise naturally as the covariance matrix of a stationary process on a planar rectangular grid. A special case, corresponding to a separable covariance function, is the Kronecker product

67

$$T = T_1 \otimes T_2 \qquad\qquad (B.2-2)$$

where T_1, T_2 are Toeplitz of dmension n_1, n_2.

Toeplitz matrices in one dimension are discussed in Appendix A, in particular the transform of a windowed $n_2 \times n_2$ Toeplitz matrix

$$T_2' = F_2 \; W_2 \; T_2 \; W_2 \; F_2^\dagger \qquad\qquad (B.2-3)$$

where W_2 is a diagonal window matrix.

The development given in Section A.2 extends directly to two dimensions. Define the $n_1 n_2 \times n_1 n_2$ diagonal window matrix W as the Kronecker product of two one-dimensional windows

$$W = W_1 \otimes W_2 \qquad\qquad (B.2-4)$$

This is a natural choice of window function on a rectangular grid. The transform of a windowed block Toeplitz matrix analogous to Eq. B.2-3 is the $n_1 n_2 \times n_1 n_2$ matrix

$$T' = F \; W \; T \; W \; F^\dagger \qquad\qquad (B.2-5)$$

where T is defined in Eq. B.2-1, W in Eq. B.2-4 and F in Eq. B.1-9.

Extend each Toeplitz block T_k in Eq. B.2-1 to a $2n_2 \times 2n_2$ circulant in the manner of Appendix A

$$\tilde{T}_k = \begin{bmatrix} T_k & R_k \\ R_k & T_k \end{bmatrix} \qquad\qquad (B.2-6)$$

If the Toeplitz matrix T_k is defined by the vector

$$\underline{t} = [t_{-(n_2-1)}, \cdots, t_{-1}, t_0, t_1, \cdots, t_{n_2-1}]^T \quad (B.2-7)$$

then R_k is the complementary Toeplitz matrix defined by

$$\underline{r} = [t_{-1}, \cdots, t_{-(n_2-1)}, \tfrac{1}{2}(t_{-(n_2-1)} + t_{n_2-1}), t_{n_2-1}, \cdots, t_1]^T$$

$$(B.2-8)$$

Now extend T to a $4n_1n_2 \times 4n_1n_2$ block circulant in the same manner

$$\tilde{T} = \begin{bmatrix} T^* & R^* \\ R^* & T^* \end{bmatrix} \quad (B.2-9)$$

where T^* is the $2n_1n_2 \times 2n_1n_2$ block Toeplitz matrix

$$T^* = \begin{bmatrix} \tilde{T}_0 & \tilde{T}_1 & \cdots & \tilde{T}_{n_1-1} \\ \tilde{T}_{-1} & \cdot & \cdot & \\ \cdot & \cdot & \cdot & \cdot \\ \tilde{T}_{-(n_1-1)} & \cdot & \cdot & \end{bmatrix} \quad (B.2-10)$$

and R^* is the complementary block Toeplitz matrix

$$R^* = \begin{bmatrix} \tfrac{1}{2}(\tilde{T}_{-(n_1-1)} + \tilde{T}_{n_1-1}) & \tilde{T}_{n_1-1} & \cdots & \tilde{T}_1 \\ \tilde{T}_{-(n_1-1)} & & \cdot & \cdot \\ \cdot & & \cdot & \cdot & \cdot \\ \tilde{T}_{-1} & & & \cdot & \cdot \end{bmatrix} \quad (B.2-11)$$

69

The extension of the window matrix and DFT to compatible size $(4n_1n_2)$ is straightforward. That is,

$$\tilde{W} = \begin{bmatrix} W & 0 \\ 0 & 0 \end{bmatrix} = \tilde{W}_1 \otimes \tilde{W}_2 \qquad (B.2\text{-}12)$$

where $\tilde{W}_1$, $\tilde{W}_2$ are one-dimensional extensions to size $2n_1$, $2n_2$, and

$$F = \tilde{F}_1 \otimes \tilde{F}_2 \qquad (B.2\text{-}13)$$

where $\tilde{F}_1$, $\tilde{F}_2$ are DFT's of size $2n_1$, $2n_2$. Thus Eq. B.2-5 can be written

$$T' = S \tilde{F} \tilde{W} \tilde{T} \tilde{W} \tilde{F} S^T \qquad (B.2\text{-}14)$$

where S is a two-dimensional sampling matrix

$$S = S_1 \otimes S_2 \qquad (B.2\text{-}15)$$

formed from two sampling matrices as defined in Appendix A. Finally,

$$T' = S \tilde{W}' \tilde{T}' \tilde{W}' S^T \qquad (B.2\text{-}16)$$

where the transformed matrices

$$\tilde{W}' = \tilde{F} \tilde{W} \tilde{F}^\dagger \quad , \quad \tilde{T}' = \tilde{F} \tilde{T} \tilde{F}^\dagger \qquad (B.2\text{-}17)$$

are block circulant and diagonal, respectively, by the theorems of Section B.1.

B.2.2 Efficient Calculation of the Transform

Equation B.2-16 is the direct analog of the one-dimensional Eq. A.2-12, and can be used to exhibit an element-by-element formula analogous to Eq. A.2-20. It is instructive to express Eq. B.2-16 in terms of the underlying one-dimensional transforms so that the one-dimensional theory can be applied. This is especially easy when the covariance function is separable, since then Eqs. B.2-2 and B.2-12 to B.2-15 show that the computation "factors" completely to

$$T' = T_1' \otimes T_2' \qquad\qquad (B.2-18)$$

where

$$T_1' = S_1 \, \tilde{W}_1' \tilde{T}_1' \tilde{W}_1' S_1^{\,T} \qquad\qquad (B.2-19)$$

is the one-dimensional transform of T_1, and similarly for T_2'. Thus only two one-dimensional transforms are required in this case, and their banded approximations may be calculated as described in Appendix A in the order of $m_B(n_1 \log_2 n_1 + n_2 \log_2 n_2)$ operations.[*]

In the non-separable case this factorization is only partial in the sense that $\tilde{T}'$ in Eq. B.2-16 does not factor into a Kronecker product. However, $\tilde{T}'$ is a diagonal matrix and can be represented as a sum of products of diagonal matrices

$$\tilde{T}' = \sum_{p=o}^{2n_1-1} \sum_{q=o}^{2n_2-1} [\mathrm{diag}(\underline{e}_p) \otimes \mathrm{diag}(\underline{e}_q)] \, \tau_{pq} \qquad\qquad (B.2-20)$$

---

[*]This assumes that both windows W_1, W_2 have the same bandwidth, m_B, which is not required.

where $\underline{e}_p$, $\underline{e}_q$ are p^{th}, q^{th} unit vectors of dimension $2n_1$, $2n_2$, and τ_{pq} are the elements of a $2n_1 \times 2n_2$ matrix containing the diagonal entries of $\tilde{T}'$. Specifically, let $\underline{\tau}$ be the $4n_1n_2$-vector corresponding row-wise to τ_{jk}. Then from Eq. B.1-20

$$\underline{\tau} = \left[\sqrt{2n_1} \; \tilde{F}_1 \otimes \sqrt{2n_2} \; \tilde{F}_2 \right]^\dagger \tilde{\underline{c}} \qquad (B.2-21)$$

where $\tilde{\underline{c}}$ is the first row of the circulant $\tilde{T}$ constructed in Eqs. B.2-6 to B.2-11. The vector $\tilde{\underline{c}}$ can be defined explicitly in terms of the first row and column of T by Eq. B.2-1.

With the representation of Eq. B.2-20 the transform Eq. B.2-16 becomes

$$T' = \sum_{p=o}^{2n_1-1} \sum_{q=o}^{2n_2-1} (A'_p \otimes B'_q) \; \tau_{pq} \qquad (B.2-22)$$

where

$$A'_p = S_1 \; \tilde{W}'_1 \; \text{diag}(\underline{e}_p) \; \tilde{W}'_1 \; S_1^T,$$

$$\qquad (B.2-23)$$

$$B'_q = S_2 \; \tilde{W}'_2 \; \text{diag}(\underline{e}_q) \; \tilde{W}'_2 \; S_2^T$$

The calculation of A'_p and B'_q is quite simple since $\text{diag}(\underline{e}_p) = \underline{e}_p \underline{e}_p^T$ implies that[*]

$$A'_p = \underline{a}_p \; \underline{a}_p^\dagger \quad , \quad \underline{a}_p = S_1 \; \tilde{W}'_1 \; \underline{e}_p \qquad (B.2-24)$$

---

[*]Note that $\tilde{W}'_1 = F_1 \; \tilde{W}_1 \; F_1$ is hermitian so that $(\tilde{W}'_1)^\dagger = \tilde{W}'_1$.

72

Furthermore, the matrix $\tilde{W}_1^!$ is a circulant whose first row is given by

$$\underline{\Omega}_1 = \frac{1}{\sqrt{2n_1}} \; \tilde{F}_1^\dagger \begin{bmatrix} \underline{w}_1 \\ 0 \end{bmatrix} \qquad\qquad (B.2-25)$$

so that the vectors $\underline{a}_p$ can all be computed with a single FFT. Explicitly,

$$a_{jp} = [\tilde{W}_1^!]_{2j,p} = \Omega_{1,p-2j} \qquad\qquad (B.2-26)$$

where negative subscripts are interpreted modulo $2n_1$, and

$$\begin{bmatrix} A_p' \end{bmatrix}_{jk} = a_{jp} \, \bar{a}_{kp} = \Omega_{1,p-2j} \, \bar{\Omega}_{1,p-2k} \qquad\qquad (B.2-27)$$

where $\bar{\Omega}_{1,j}$ is the complex conjugate of $\Omega_{1,j}$.

Since $\underline{\Omega}_1$ is the transform of the window $\underline{w}_1$ the matrix A_p' is approximately banded with bandwidth m_B (see Appendix A). The representation of Eq. B.2-22 then shows that the matrix T' is approximated by a block-banded matrix (with banded blocks) when A_p' and B_q' are replaced by their (one-dimensional) banded approximations. This follows from the fact that the Kronecker product of banded matrices is block-banded (see Eq. B.1-7), and that this property is preserved under addition. The total number of non-zero elements in the block-banded form of T' is less than $(2m_B+1)^2 N$, and for each row j ($0 \le j \le N-1$) the band elements occur in the columns $j \pm m$ where $m = m_1 n_2 + m_2$ ($0 \le m_1$, $m_2 \le m_B$).

The elements of T' may be efficiently computed bandwise as in the one-dimensional case. In fact if $j = j_1 n_2 + j_2$ then

$$[T']_{j,j+m} = \sum_{p=o}^{2n_1-1} \sum_{q=o}^{2n_2-1} \alpha_{p-2j_1}(m_1) \, \beta_{q-2j_2}(m_2) \, \tau_{pq} \tag{B.2-28}$$

where $\quad 0 \le j_1 \le n_1 - 1 \quad , \quad 0 \le j_2 \le n_2 - 1, \quad$ and

$$\begin{aligned}
\alpha_k(m) &= \Omega_{1,k} \, \bar{\Omega}_{1,k-2m} \\
\beta_k(m) &= \Omega_{2,k} \, \bar{\Omega}_{2,k-2m}
\end{aligned} \tag{B.2-29}$$

The analogy with the one-dimensional formula is completed by defining

$$\underline{\rho}(m) = \underline{\alpha}(m_1) \otimes \underline{\beta}(m_2) \tag{B.2-30}$$

so that

$$[T']_{j,j+m} = \sum_{\ell=o}^{4n_1n_2-1} \rho_{\ell-2j}(m) \, \tau_\ell \tag{B.2-31}$$

where $\underline{\tau}$ is defined by Eq. (B.2-21). Equation B.2-28 can be recognized as a convolution or circulant multiplication (see Eq. B.1-29) and can therefore be computed in the order of $N\log_2 N$ operations. The total workload to compute all bands in the approximation is therefore of order $m_B^2 \, N\log_2 N$.

In practice the complex transforms implied by Eqs. B.2-25 and B.2-29 are replaced by real transforms. This amounts to replacing the complex DFT matrix F in Eq. B.2-5 by the real DFT matrix HF where

$$H = H_1 \otimes H_2 \tag{B.2-32}$$

74

is a complex $n_1n_2 \times n_1n_2$ matrix, and H_1, H_2 are equal to the
matrix H defined in Appendix A (Eq. A.3-2) for $n = n_1$, n_2.
Similarly, $F^\dagger$ is replaced by $F^\dagger H^\dagger$ so that Eq. B.2-5 is formal-
ly identical to Eq. A.3-1. The result is that the banded blocks
of T' have the structure described for the one-dimensional
case in Appendix A.

B.3 APPROXIMATE SOLUTION OF BLOCK TOEPLITZ EQUATIONS

  B.3.1 Fast Multiplication

        There are two possible ways to obtain a "fast" multi-
plication algorithm for block Toeplitz matrices, both of which
are of order $Nlog_2N$ in complexity. The simplest method is the
application of fast convolution (Section B.1.2) to the circulant
matrix $\tilde{T}$ (Eq. B.2-9) as described in Ref. 10 for one dimension.
This method is rejected here since experience with the one-
dimensional algorithm has shown that estimation errors are
poorly behaved with this technique. The reason is that the
consistency in the statistical modelling (Ref. 13), which im-
plicitly defines the relation between the estimates and the
data, is destroyed if the auto-covariance is band-approximated
(see Section B.3.2) and the cross-covariance is not.

        Therefore, it is assumed that the matrix to be multi-
plied is replaced by its block-banded approximation. A straight-
forward block-banded multiplication algorithm then requires on
the order of $m_B^2 N$ operations, in addition to computing the approx-
imation, since the total number of non-zero elements in a row
is m_B^2. The workload is thus still dominated by $m_B^2 Nlog_2N$.

B.3.2 Fast Inversion of Separable Matrices

Consider the linear system

$$\underline{y} = T \, \underline{x} \qquad\qquad (B.3\text{-}1)$$

where T is block Toeplitz of dimension $n_1 n_2 \times n_1 n_2$. Its frequency domain counterpart is

$$\underline{y}' = T'\underline{x}' \qquad\qquad (B.3\text{-}2)$$

where

$$\underline{y}' = A \, \underline{y} \quad , \quad \underline{x} = A^\dagger \underline{x}'$$
$$T' = A \, T \, A^\dagger \qquad\qquad (B.3\text{-}3)$$

and A is the transformation matrix defined by

$$A = H \, F \, W \qquad\qquad (B.3\text{-}4)$$

where H, F, and W are defined in Section B.2. The solution of Eq. B.3-1 for $\underline{x}$ reduces to the solution of Eq. B.3-2 for $\underline{x}'$.

If T is separable and symmetric then from Eq. B.2-18

$$\underline{y}' = (T_1' \otimes T_2') \, \underline{x}' \qquad\qquad (B.3\text{-}5)$$

or using Eqs. B.1-10 and B.1-11

$$\underline{x}' = [(T_1')^{-1} \otimes (T_2')^{-1}] \, \underline{y}' \qquad\qquad (B.3\text{-}6)$$

$$X' = (T_1')^{-1} \, Y' (T_2')^{-1} \qquad\qquad (B.3\text{-}7)$$

where $\underline{x}'$, $\underline{y}'$ are the row-wise elements of the $n_1 \times n_2$ matrices X', Y'. Equation B.3-7 can be further expanded to two simple

matrix inversions

$$V' = (T_2')^{-1}(Y')^T$$

$$\text{(B.3-8)}$$

$$X' = (T_1')^{-1}(V')^T$$

Since T_1', T_2' are one-dimensional transforms of Toeplitz matrices they may be replaced by their banded approximations and inverted by the Cholesky method as described in Appendix A. However, the right-hand-sides of Eq. B.3-8 are now matrices, resulting in a workload for both equations of order

$$q = m_B n_2 (m_B + n_1) + m_B n_1 (m_B + n_2) \qquad \text{(B.3-9)}$$

where m_B is the bandwidth of the approximation. If $n_1 = n_2$ then q is of order $2m_B N$.

B.3.3 Iterative Solution for Nonseparable Matrices

When the matrix T is not separable the transform T' cannot be expressed as a Kronecker product. However, there exists a natural approximation to T which is separable, and may be used as the basis for an iterative technique. If T is a symmetric block Toeplitz matrix (Eq. B.2-1) it is defined by the sequence of vectors

$$\underline{t}_k = [t_{-(n_2-1),k}, \ldots, t_{ok}, \ldots, t_{n_2-1,k}]^T \qquad \text{(B.3-10)}$$

which in turn define the blocks T_k for k = 0, 1, ..., n_1-1. The matrix T is separable if

$$\underline{t}_k = s_k \underline{t}_o \qquad \text{(B.3-11)}$$

77

since then $T = S_o \otimes T_o$ where S_o is a symmetric Toeplitz matrix defined by the vector

$$\underline{s}_o = [1, s_1, \quad \cdots \quad , s_{n_1-1}] \qquad \text{(B.3-12)}$$

A natural Kronecker approximation is obtained by choosing $s_k = t_{ok}/t_{oo}$. With this choice the approximation agrees with T identically for the main diagonal block T_o, and for the main diagonal within each block T_k. The error in the approximation is determined by Eq. B.3-11.

Let $D = S_o \otimes T_o$ and express T as

$$T = D + E$$

where E is the error in the separable matrix approximation. Since T and D are Toeplitz so is E, being defined by the vectors

$$\underline{e}_k = \underline{t}_k - s_k \underline{t}_o \qquad \text{(B.3-13)}$$

The transformed linear system (Eq. B.3-2) becomes

$$\underline{y}' = (D' + E') \, \underline{x}' \qquad \text{(B.3-14)}$$

where D' is the Kronecker product $S_o' \otimes T_o'$, and $E' = T' - D'$.

An iterative solution to Eq. B.3-14 can be based on the identity

$$\underline{x}' = (D')^{-1} [\underline{y}' - E' \underline{x}'] \qquad \text{(B.3-15)}$$

which leads to the recursion

$$\underline{x}'(k+1) = (D')^{-1}[\underline{y}' - E' \underline{x}'(k)] \qquad (B.3\text{-}16)$$

where k is the iteration step number and $\underline{x}'(0)$ is any conven-
ient initial solution (perhaps the zero vector). Since D' may
be inverted in order $m_B N$ operations from Section B.3.2, and
the multiplication by E' carried out in order $m_B^2 N$ from Section
B.3.1, the workload represented by Eq. B.3-16 is of order $m_s m_B^2 N$
where m_s is the number of iteration steps.

Iterative methods for linear systems are discussed in
Ref. 12. The recursion, Eq. B.3-16, converges to the solution
$\underline{x}'$ of Eq. B.3-14 if the approximation D' is sufficiently close
to T'. Let

$$\delta\underline{x}'(k) = \underline{x}'(k)-\underline{x}' \qquad (B.3\text{-}17)$$

be the error in the kth iterate. Then

$$\delta\underline{x}'(k) = M^k \, \delta\underline{x}'(0) \quad , \quad M = (D')^{-1}E' \qquad (B.3\text{-}18)$$

and the iteration converges if any matrix norm of M is less
than one, in particular if the eigenvalues of M are all less
than one in absolute value. An expression for the convergence
rate in terms of the number of steps, m_s, required to reduce
the initial error by $10^{-\beta}$ is given by

$$m_s = \frac{\beta}{-\log_{10}\rho} \quad , \quad \rho = \max_i \left| \lambda_i(M) \right| \qquad (B.3\text{-}19)$$

where $\lambda_i(M)$ denotes the eigenvalues of the matrix M. For a
useful algorithm m_s should be less than 10 when $\beta = 2$.

Since both T' and D' are normally symmetric and posi-
tive definite, a simpler convergence criterion is (Ref. 12) that

$$(2D'-T') \equiv D'(I-M) \qquad (B.3-20)$$

is a positive definite matrix. This holds when the Toeplitz matrix (2D-T) is itself positive definite, or in particular if

$$\max_{i}\left|\lambda_{i}(T)\right| < 2\,\min_{i}\left|\lambda_{i}(S_{o})\right| \cdot \min_{i}\left|\lambda_{i}(T_{o})\right| \qquad (B.3-21)$$

since D is a Kronecker product. In this case the rate of convergence can be estimated using Eq. B.3-19 and the inequalities

$$\min_{j}\,\left|\lambda_{j}(T)\right|/\max_{j}\,\left|\lambda_{j}(D)\right| < 1 + \lambda_{i}(M) < \max_{j}\,\left|\lambda_{j}(T)\right|/\min_{j}\,\left|\lambda_{j}(D)\right|$$

$$(B.3-22)$$

The convergence of the iteration can be guaranteed, and an optimum rate of convergence obtained, by introducing a relaxation parameter, α. Let $D = \alpha^{-1}D_{o}$ where $D_{o} = S_{o} \otimes T_{o}$ and α is a positive real number. Then (2D-T) is a positive-definite matrix for sufficiently small α so that convergence is assured. Substitution shows that Eq. B.3-16 can be rewritten

$$\underline{x}'(k+1) = \underline{x}'(k) + \alpha(D_{o}')^{-1}\,[\underline{y} - T'\underline{x}'(k)] \qquad (B.3-23)$$

which is in the form of a relaxation iteration.

Analysis of the convergence rate of Eq. B.3-23 shows that the optimum choice of α is given by

$$\alpha_{o} = 2(q_{1} + q_{2})^{-1} \qquad (B.3-24)$$

where q_{1} and q_{2} are the smallest and largest eigenvalues of $(D_{o}^{-1}T)$. The q's may be estimated from upper and lower bounds for the real, positive ratio $\underline{x}^{T}T\underline{x}/\underline{x}^{T}D_{o}\underline{x}$. The convergence factor corresponding to Eq. B.3-24 is given by

$$\rho_o = (q_2 - q_1)/(q_2 + q_1) \qquad\qquad (\text{B.3-25})$$

which is less than one for any T, and reaches zero in the separable case $T = D_o$. The number of steps required to reduce the error by a factor of 100 (see Eq. B.3-19) is less than ten when the condition number of $(D_o^{-1}T)$, given by q_2/q_1, is less than about five. Furthermore, it can be shown that the number of steps increases linearly with the condition number.

REFERENCES

1. Akaike, H., "Block Toeplitz Matrix Inversion," _SIAM J. Appl. Math._, Vol. 24, 1973, pp. 234-241.

2. Bellman, R., _Introduction to Matrix Analysis_, McGraw-Hill, New York, 1960.

3. Brace, K.L., and Shultz, M.E., "Ocean-Area Geoid Heights and Mean Gravity Anomalies from GEOS-3 Data," Defense Mapping Agency Aerospace Center, St. Louis A.F. Station, Mo., October 1978.

4. Cooley, J.W., Lewis, P.A.W., and Welch, P.D., "The Fast Fourier Transform and Its Applications," Report No. RC-1743, IBM Watson Research Center, Yorktown Heights, New York, 1967.

5. Cooley, J.W., and Tukey, J.W., "An Algorithm for the Machine Calculation of Complex Fourier Series," _Math. of Comp._, Vol. 19, 1965, pp. 297-301.

6. Forsythe, G.E., and Moler, C.B., _Computer Solution of Linear Algebraic Systems_, Prentice-Hall, Englewood Cliffs, New Jersey, 1967.

7. Gilbert, E.N., "Distortion in Maps," _SIAM Rev._, Vol. 16, 1974, pp. 47-62.

8. Harris, F.J., "On the Use of Windows for Harmonic Analysis with the Discrete Fourier Transform," _IEEE Proceedings_, Vol. 66, 1978, pp. 51-83.

9. Heiskanen, W.A., and Moritz, H., _Physical Geodesy_, W.H. Freeman and Co., 1967.

10. Heller, W.G., Tait, K.S., and Thomas, S.W., "GEOFAST - A Fast Gravimetric Estimation Algorithm," The Analytic Sciences Corporation, Report No. AFGL-TR-77-0195, August 1977.

11. Heller, W.G., and Jordan, S.K., "Attenuated White Noise Statistical Gravity Model," _J. Geophys. Res._, Vol. 84, 1979, pp. 4680-4688.

12. Isaacson, E., and Keller, H.B., _Analysis of Numerical Methods_, Wiley, New York, 1966.

REFERENCES (Continued)

13.   Jordan, S.K., "Self-Consistent Statistical Models for
       the Gravity Anomaly, Vertical Deflections, and Undula-
       tion of the Geoid," J. Geophys. Res., Vol. 77, 1972,
       pp. 3660-3670.

14.   Justice, J.H., "An Algorithm for Inverting Positive Def-
       inite Toeplitz Matrices," SIAM J. Appl. Math., Vol. 23,
       1971, pp. 289-291.

15.   Kaiser, J.F., "Nonrecursive Digital Filter Design Using
       the I_o-SINH Window Function," Proc. 1974 IEEE Int. Symp.
       on Circuits and Syst., April 1974, pp. 20-23.

16.   Levinson, N., "The Wiener rms (Root Mean Square) Error
       Criterion in Filter Design and Prediction," J. Math.
       Phys., Vol. 25, 1947, pp. 261-278.

17.   Moritz, H., "Advanced Least-Squares Methods," Report
       No. 175, Dept. of Geod. Sci., Ohio State University,
       Columbus, Ohio, 1972.

18.   Pratt, W.K., "Generalized Wiener Filter Computation Tech-
       niques," IEEE Trans. on Computers, Vol. C-21, July 1972,
       pp. 636-641.

19.   Rabiner, L.R., and Gold, B., Theory and Application of
       Digital Signal Processing, Prentice Hall, Englewood
       Cliffs, New Jersey, 1975.

20.   Stockham, T.G., "High-Speed Convolution and correlation,"
       1966 Spring Joint Computer Conference, AFIPS Proc, Vol.
       28, pp. 228-233.

21.   Tait, K.S., "A Fast Gravimetric Estimation Technique,"
       Proc. 1978 Position, Location and Navigation Symp.,
       November 1978, pp. 89-93.

22.   Thomas, S.W., and Heller, W.G., "Efficient Estimation
       Techniques for Integrated Gravity Data Processing," The
       Analytic Sciences Corporation, Report No. AFGL-TR-76-0232,
       September 1976.

23.   Trench, W., "An Algorithm for the Inversion of Finite
       Toeplitz Matrices," SIAM J. Appl. Math., Vol. 12, 1964,
       pp. 515-522.

REFERENCES (Continued)

24.   Tscherning, C.C., and Rapp, R.H., "Closed Covariance
       Expressions for Gravity Anomalies, Geoid Undulations,
       and Deflections of the Vertical Implied by Anomaly De-
       gree Variance Models," Report No. 208, Dept. of Geod.
       Sci., Ohio State University, Columbus, Ohio, 1974.

E

ED

80